Vibronic emission from short-lived core-hole states: Theory and applications for the water molecule

Amary Cesar and Hans Ågren
Institute of Quantum Chemistry, University of Uppsala, P.O.B. 518, S-75120 Uppsala, Sweden

Vincenzo Carravetta
Istituto di Chimica Quantistica ed Energetica Molecolare del Consiglio Nationale delle Ricerche, Via Risorgimento 35, 56100 Pisa, Italy

(Received 3 June 1988; revised manuscript received 1 February 1989)

Vibronic cross sections for x-ray and Auger decay from short-lived core-hole states in molecules are derived starting from Åberg's description of atomic x-ray and Auger decay as multichannel-scattering processes [Åberg, Phys. Scr. **21**, 495 (1980)]. The derivation includes a scattering-matrix formulation in which intra- and interchannel interactions as well as nonadiabatic corrections are introduced. Computable expressions for x-ray and Auger vibronic spectra are derived assuming the harmonic approximation for multidimensional nuclear motions. Applications for water are carried out using truly *ab initio* values for all energy and lifetime-related parameters.

I. INTRODUCTION

Modern atomic theory formulates the Auger and x-ray emission effects in terms of multichannel–resonance-scattering processes[1] along the ideas originally outlined by Fano[2] and Feshbach.[3] The extension of this view to molecular systems is feasible although the introduction of additional degrees of freedom due to the nuclear motion certainly makes the theory more complicated, since it then is necessary to handle many electronically bound vibronic states that simultaneously interact with many vibronically open channels.

The theory of nuclear dynamics and vibronic spectra involving short-lived electronic states has mostly been associated with the interpretation of resonant electron-molecule scattering experiments.[4] Since the proposal of the "boomerang model" by Birtwistle and Herzenberg,[5] considerable theoretical effort has been devoted to this problem.[4] The more elaborated formulations, such as the Feshbach projection-operator method,[6–8] or configuration interaction in the continuum states,[9,10] of electron-molecule scattering cross sections for vibrational excitation and dissociative attachment lead to complex energy-dependent and nonlocal potentials for the nuclear motion in the resonance state. Much of the theory of electron-molecule scattering can be associated with vibronic emission spectra of short-lived inner-vacancy states, provided the excitation of the molecule and the subsequent decay is treated as a single quantum-mechanical process.

Due to the development of high-resolution x-ray and Auger spectroscopy, the effect of lifetime-vibrational interference in vibronic decay of molecular core-hole states has now been firmly established.[11–16] In contrast to absorption spectra, viz., photoionization and electron-energy loss spectra, in which the finite lifetime manifests itself merely as a broadening of vibronic components, the corresponding emission spectra may exhibit significant constructive or destructive lifetime-vibrational interference. Several theoretical studies have been devoted to this effect. Gel'mukhanov *et al.*[11,12] started out from the Kramer-Heisenberg dispersion formula and derived an effective one-particle Green's function for the x-ray cross sections; Kaspar *et al.*[13] carried out a derivation that utilizes a scattering S matrix and vibronic coupling constants, while Correia *et al.*[14] derived the vibronic cross sections for x-ray and Auger emission by means of a time-dependent Franck-Condon formulation. Common for these theoretical investigations is the assumption of non-post-collisional interaction (non-PCI), the Born-Oppenheimer (BO) approximation, and the local approximations for the nuclear Hamiltonian. In all numerical applications so far the lifetime of the core-hole state has been used as a prefixed parameter and, just as the electronic transition moments, assumed to be constant for all nuclear conformations.

In the present work we start out from Åberg's formulation of atomic x-ray and Auger decay as multichannel–resonance-scattering processes[1] and make a generalization of this formulation to systems with nuclear degrees of freedom. We derive vibronic cross sections for molecular x-ray and Auger emission where inter- and intrachannel interactions, nonadiabatic corrections, correlation, and many-body interactions may be introduced at progressively more sophisticated levels of approximation. The possibility of doing so actually results as the main advantage of using Åberg's general scattering formulas as a starting point rather than, e.g., the Feshbach projection-operator approach, and constitutes an important motivation for the present work. For the numerical applications we derive working equations that assume the non-PCI, BO, and the local approximations, but including the full effect of finite lifetime, variations of lifetime, and electronic transition moments with nuclear geometry, and the discrete continuum-interaction energy

shift. The treatment of nuclear motion is performed multidimensionally within the harmonic approximation. This implies the inherent advantage that full analyticity can be maintained for the cross sections at gradually coarser levels of approximation in the vibronic analysis. These levels of approximation here refer to use of vibronic coupling constants and the use of diagonal or full transformation matrices between normal coordinates of the different electronic states. In all cases we have made complete nonempirical constructions of the vibronic spectra, i.e., all underlying parameters are obtained *ab initio* either here or from our recent published work; force fields, x-ray moments, photoelectron moments (this work), partial Auger rates and lifetime,[17] lifetime nuclear variation,[18] and energy shift.[19] In the application for x-ray and Auger spectra bands of water, we have investigated the relative importance of these parameters and also the role of different approximations for the normal coordinate transformations.

II. METHOD

Following the ideas behind Åberg's[1] resonant-scattering theory formulation of atomic Auger and x-ray processes our aim is to get the total Hamiltonian $\hat{H}$ of a system formed by one molecule and a radiation field diagonalized in a small state-vector space containing four basic elements: $|i\omega\rangle$, $|\phi e_1\rangle$, $|Ae_1e_2\rangle$, and $|xe_1\omega_x\rangle$. The first of these state vectors $|i\omega\rangle$ represents the molecule in its initial electronic ground state and a photon carrying an energy $\hbar\omega$ and linear momentum k. After having absorbed one photon with sufficient energy for core-electron ionization, the system is described by the final-state vector identified either as $|Ae_1e_2\rangle$, a doubly ionized molecule in an electronic state A, and two electrons e_1 and e_2 in the continuum or $|xe_1\omega_x\rangle$, a singly ionized molecule in an electronic state x, an electron in the continuum e_1, and an x-ray photon carrying an energy ω_x and linear momentum k_x. These final states represent the product from a direct or, alternatively, from a resonant-scattering event involving an intermediate state represented by the state vector $|\phi e_1\rangle$. This state contains information about the residual core-hole molecular species in the electronic state ϕ and a single (primary) escaping photoelectron with energy $\varepsilon_{e_1}=\omega-I_\phi$. I_ϕ is the threshold energy for the ϕ^{th} ionization potential of the neutral molecule. The energies of the (secondary) Auger electron ε_{e_2} and the x-ray photon are characteristics of the emitting molecular ion possessing the nominal values $\varepsilon_{e_2}=I_\phi-I_A$ and $\omega_x=I_\phi-I_x$, respectively. I_A and I_x have a meaning equivalent to I_ϕ.

For the simplicity of treatment we assume here that the resonant event proceeds through a single energetically selected intermediate core-hole state isolated from all other near-lying neighbors, as the higher-lying members of a limiting Rydberg series, for instance. Also, the analysis will be performed with the underlying assumption that the excess of energy carried by the primary photoionized electron e_1 is high enough to prevent any appreciable PCI effects[20] between this photoelectron and any of the particles involved in the decay processes. This assumption allows us to define a one-electron state vector $|e_1\rangle$, strongly orthogonal to $|\phi\rangle$, $|Ae_2\rangle$, and $|x\omega_x\rangle$, and to write the state vectors that contain the primary photoelectron e_1 as a direct product of state vectors as[21] $|\phi e_1\rangle=|\phi\rangle\otimes|e_1\rangle$, $|Ae_1e_2\rangle=|Ae_2\rangle\otimes|e_1\rangle$, and $|xe_1\omega_x\rangle=|x\omega_x\rangle\otimes|e_1\rangle$.

It proves to be convenient to divide the state-vector space in two interacting subspaces. The subspace I, the so-called resonant space, will contain only one bound-state vector, namely $|\phi e_1\rangle$, while the subspace II, the background continuum or simply the background, will be spanned by the scattering-state vectors $|i\omega\rangle$, $|xe_1\omega_x\rangle$, and $|Ae_1e_2\rangle$ having at most one particle in the continuum. We do not include any rotational degree of motion or rotational interactions in the present study, which is justified by the fact that the rotational time involved in the studied processes is admittedly large compared with the vibrational and/or electronic time scales. The final cross sections of Eqs. (15) and (18) should thus be interpreted as cross sections for scattering of a particle or a molecule with a fixed orientation in space, averaged over all directions and integrated for all directions of the emitted particle. In cases where photons are participating in the scattering process either as an incoming or as an emitted particle, we should also sum over the initial and average over the final polarizations states. Accordingly, in what follows, we will be able to completely specify the continuum part of the system by just using one label; the excess of energy $\varepsilon=\varepsilon_\alpha=\frac{1}{2}k_\alpha^2$ carried by the particle in the continuum relative to the total energy of the residual molecular species that defines the αth open channel.

Now, let the wave functions $\psi'_{\alpha\varepsilon}(\mathbf{r},\mathbf{R})$ ($\alpha=i,x,A$) and $\phi'(\mathbf{r},\mathbf{R})$ be the spatial coordinate representations of the state vectors belonging to the background and the resonant subspaces, respectively, where $\mathbf{r}$ stands collectively for the spatial coordinates of all electrons and $\mathbf{R}$ for the nuclear coordinates. We impose the Born-Oppenheimer (BO) adiabatic approximation for these wave functions which means that they are factorizable as a product of an electronic wave function, functionally depending on $\mathbf{r}$ and parametrically on $\mathbf{R}$, and a nuclear wave function depending only on $\mathbf{R}$, i.e.,

$$\psi'_{\alpha\varepsilon}(\mathbf{r},\mathbf{R})=\psi_{\alpha\varepsilon}(\mathbf{r};\mathbf{R})\chi_\alpha(\mathbf{R})$$

and

$$\phi'(\mathbf{r},\mathbf{R})=\phi(\mathbf{r};\mathbf{R})\Upsilon(\mathbf{R})\ .$$

The set $\{\chi_\alpha\}$ of nuclear wave functions is assumed to form a complete set of orthonormalized functions for each given α [the intermediate state nuclear wave function $\Upsilon(\mathbf{R})$ is specified later]. To completely specify the above wave functions we choose the scattering functions $\psi'_{\alpha\varepsilon}(\mathbf{r},\mathbf{R})$ fulfilling the boundary condition for standing scattering waves

$$\psi_{\alpha\varepsilon}(\mathbf{r};\mathbf{R})\chi_\alpha(\mathbf{R})\underset{r\to\infty}{\sim}\frac{\Omega_\alpha(\mathbf{r}',\mathbf{R})\chi_\alpha(\mathbf{R})}{r\sqrt{k_\alpha}}\sin[k_\alpha r+\delta_\alpha(\varepsilon)]\ , \tag{1}$$

while the resonant wave function must have a vanishing limit because it represents a bound-state function, i.e.,

$$\phi(\mathbf{r},\mathbf{R})\Upsilon(\mathbf{R})\rightarrow 0 \quad \text{as } r\rightarrow\infty \ . \tag{2}$$

We have used $\Omega_\alpha(\mathbf{r}';\mathbf{R})$ for the wave function of the electronic discrete state of the molecular residual species defining the αth channel, $r\ (=|\mathbf{r}|)$ and $\mathbf{r}'$ for the spatial coordinates of the escaping particle and the remaining molecular bound electrons, respectively, and $\delta_\alpha(\varepsilon)$ for a phase shift related to the scattering process.

The set $\{\{\psi'_{\alpha\varepsilon}(\mathbf{r},\mathbf{R})\},\phi'(\mathbf{r},\mathbf{R})\}$, is, in general, a set of nonorthogonal and interacting functions with respect to the total Hamiltonian operator $\hat{H}$. On the other hand, we can form the set of functions $\{\{\Psi^{\pm}_{\alpha\varepsilon}(\mathbf{r},\mathbf{R})\},\phi'(\mathbf{r},\mathbf{R})\}$ which has the remarkable property of being noninteracting with respect to the operator $(\hat{H}-E)$ within the background subspace of functions $\{\Psi^{\pm}_{\alpha\varepsilon}(\mathbf{r},\mathbf{R})\}$. These functions,

$$\Psi^{\pm}_{\alpha\varepsilon}(\mathbf{r},\mathbf{R})=\psi_{\alpha\varepsilon}(\mathbf{r};\mathbf{R})\chi_\alpha(\mathbf{R}) + \sum_\beta\sum_{n_\beta}\lim_{\nu\rightarrow 0}\int d\varepsilon'\frac{\psi_{\beta\varepsilon'}(\mathbf{r};\mathbf{R})\chi_\beta(\mathbf{R})Y^{\pm}_{\beta\alpha}(\varepsilon',\varepsilon)}{E-\mathcal{E}_\beta-\varepsilon'\pm i\nu} \tag{3}$$

formed as a linear combination of standing waves, satisfy the outgoing or incoming scattering-wave boundary conditions for $\mathcal{E}_\alpha+\varepsilon=E$[1]. The sum $\sum_\beta$ is over all electronic discrete states of the final ions or the initial neutral molecule and $\sum_{n_\beta}$ is over all nuclear vibrational levels associated with the βth electronic state with the BO vibronic energy $\mathcal{E}_\beta$ (for simplicity of notation the dependence on n_β is included in the single indices β). E is the total energy of the system (molecule plus radiation field), and the limiting procedure applies to the equality

$$\lim_{\nu\rightarrow 0}\frac{f(x)}{(x+x_0\pm i\nu)}=\mathbf{P}\frac{f(x)}{(x-x_0)}\mp i\pi f(x_0) \ ,$$

where P denotes the Cauchy principal value of the integral. $Y^{\pm}_{\beta\alpha}(\varepsilon',\varepsilon)$, present in the second term of the right-hand side of Eq. (3), is an element of the generalized nonresonant transition matrix satisfying the Lippmann-Schwinger[22] equation

$$Y^{\pm}_{\beta\alpha}(\varepsilon',\varepsilon)=\langle\chi_\beta(\mathbf{R})|\tilde{V}_{\beta\alpha}(\varepsilon',\varepsilon)|\chi_\alpha(\mathbf{R})\rangle+\sum_\gamma\sum_{n_\gamma}\lim_{\nu\rightarrow 0}\int d\tau\frac{\langle\chi_\beta(\mathbf{R})|\tilde{V}_{\beta\gamma}(\varepsilon',\tau)|\chi_\gamma(\mathbf{R})\rangle Y^{\pm}_{\gamma\alpha}(\tau,\varepsilon)}{E-\mathcal{E}_\gamma-\tau\pm i\nu} \ . \tag{4}$$

The interaction matrix element $\tilde{V}_{\beta\alpha}(\varepsilon',\varepsilon)$ in Eq. (4) is defined by

$$(\psi_{\beta\varepsilon'}|\hat{H}-E|\psi_{\alpha\varepsilon})=(\tilde{H}_\alpha+\varepsilon-E)\delta_{\alpha\beta} \times\delta(E_\alpha(\mathbf{R})+\varepsilon-E_\beta(\mathbf{R})-\varepsilon') + \tilde{V}_{\beta\alpha}(\varepsilon',\varepsilon) \ . \tag{5}$$

It should be noted that $\tilde{V}_{\beta\alpha}(\varepsilon',\varepsilon)$ operates on the space of the nuclear coordinates since, in principle, it contains not only the interaction part of the electronic Hamiltonian but also nonadiabatic corrections $(\psi_{\beta\varepsilon'}|\hat{T}|\psi_{\alpha\varepsilon})-\delta_{\beta\alpha}\delta[E_\beta(\mathbf{R})+\varepsilon'-E_\alpha(\mathbf{R})-\varepsilon]\hat{T}$ [parentheses (|) are used to represent integrations over the electronic coordinates and the angle brackets, $\langle\ |\ \rangle$, are reserved for integrations over the nuclear coordinates]. $\tilde{H}_\alpha=\hat{T}+E_\alpha(\mathbf{R})$ is here the nuclear BO Hamiltonian defined for the channel α and $\hat{T}$ is the nuclear kinetic energy operator.

Having performed the diagonalization of $(\hat{H}-E)$ within the background subspace, we now want to proceed in an analogous way with the diagonalization for the whole working state-vector space. Let the interaction matrix element between the resonant wave function ϕ and the βth one belonging to the background space be

$$\tilde{M}^{\pm}_\beta(\varepsilon',E)=(\phi|\hat{H}-E|\Psi^{\pm}_{\beta\varepsilon'}) \ . \tag{6}$$

Note that this quantity, like $\tilde{V}_{\beta\alpha}(\varepsilon',\varepsilon)$, also is an operator on the space of the nuclear coordinates. To effect the desired diagonalization, a new linear combination of functions

$$\Phi^{\pm}_{\alpha E}(\mathbf{r},\mathbf{R})=\phi(\mathbf{r};\mathbf{R})\Upsilon^{\pm}_{\alpha E}(\mathbf{R}) + \sum_\beta\sum_{n_\beta}\int d\varepsilon'\,\Psi^{\pm}_{\beta\varepsilon'}(\mathbf{r},\mathbf{R})B^{\pm}_{\beta\alpha}(\varepsilon',E) \tag{7}$$

is then formed. Again, from the requirement that the stationary Schrödinger equation and the boundary conditions for the bound $\phi(\mathbf{r};\mathbf{R})$ and scattering waves $\Psi^{\pm}_{\beta\varepsilon'}(\mathbf{r},\mathbf{R})$ and $\Phi^{\pm}_{\alpha E}(\mathbf{r},\mathbf{R})$ are satisfied, we obtain the resonant wave functions

$$\Phi^{\pm}_{\alpha E}(\mathbf{r},\mathbf{R})=\phi(\mathbf{r};\mathbf{R})\Upsilon^{\pm}_{\alpha E}(\mathbf{R})+\Psi^{\pm}_{\alpha\varepsilon}(\mathbf{r},\mathbf{R})+\sum_\beta\sum_{n_\beta}\lim_{\nu\rightarrow 0}\int d\varepsilon'\frac{\Psi^{\pm}_{\beta\varepsilon'}(\mathbf{r},\mathbf{R})\langle[\tilde{M}^{\pm}_\beta(\varepsilon',E)]^\dagger|\Upsilon^{\pm}_{\alpha E}(\mathbf{R})\rangle}{E-\mathcal{E}_\beta-\varepsilon'\pm i\nu} \tag{8}$$

together with $\Upsilon^{\pm}_{\alpha E}(\mathbf{R})$, the wave equation that governs the nuclear dynamics of the system in the intermediate state $|\phi e_1\rangle$;

$$[E-\tilde{H}_{\varphi}(\varepsilon_{e_1})-\tilde{F}^{\pm}(E)]|\Upsilon^{\pm}_{\alpha E}(\mathbf{R})\rangle=|\tilde{M}^{\pm}_{\alpha}(\varepsilon,E)\rangle \ . \tag{9}$$

The above Eq. (9) contains a complex, energy-dependent, nonlocal operator $\tilde{F}^{\pm}(E)$ defined by

$$\tilde{F}^{\pm}(E)=\sum_{\beta}\sum_{n_\beta}\lim_{\nu\to 0}\int d\varepsilon'\frac{\tilde{M}^{\pm}_{\beta}(\varepsilon',E)[\tilde{M}^{\pm}_{\beta}(\varepsilon',E)]^{\dagger}}{E-\mathcal{E}_{\beta}-\varepsilon'\pm i\nu}$$

$$=\tilde{\Delta}(E)\mp\frac{i}{2}\tilde{\Gamma}(E) \ . \tag{10}$$

The terms present in these two last equations are conveniently interpreted if we consider background outgoing waves $\Psi^{+}_{\alpha\varepsilon}(\mathbf{r},\mathbf{R})$ for the initial scatterng state i, hereafter renamed α, and incoming waves $\Psi^{-}_{\alpha\varepsilon}(\mathbf{r},\mathbf{R})$ for the final scattering states[23] $\beta(=a,x)$ for the evaluation of the $\tilde{F}(E)$ operator of Eq. (10). Accordingly, $\tilde{M}^{+}_{\alpha}(\varepsilon,E)$, is interpreted as a source of probability which steadily feeds the intermediate vibronic population from the initial vibronic scattering state α while the imaginary part of $\tilde{F}(E)$, the operator $\frac{1}{2}\tilde{\Gamma}(E)$, is associated to the decay rate of the intermediate state ϕ to alternative final channels β. Experimentally $\tilde{\Gamma}(E)$ should correspond to the width of a band associated to the intermediate state in an excitation-type spectra. The $\Delta(E)$ term causes shifts on the intermediate state BO potential energy surface so that the stationary vibrational states of the intermediate electronic state rather should be evaluated according to the modified energy-dependent BO potential surface $\tilde{E}_r=E_{\phi}+\varepsilon_{e_1}+\tilde{\Delta}(E)$.

The resonant-transition matrix $\underline{\mathcal{T}}$, which is derived along with the procedure that led to Eq. (8), assumes a simpler form if the final scattering states β are represented by an incoming wave boundary condition and, as before, the initial scattering state α by the outgoing wave boundary condition. Explicitly, we have

$$\mathcal{T}_{\beta\alpha}(\varepsilon',\varepsilon,E)=\mathcal{T}^{\text{nonres}}_{\beta\alpha}(\varepsilon',\varepsilon,E)+\langle[\tilde{M}^{-}_{\beta}(\varepsilon',E)]^{\dagger}|[E-\tilde{H}_{\phi}(\varepsilon_{e_1})-\tilde{F}(E)]^{-1}|\tilde{M}^{+}_{\alpha}(\varepsilon,E)\rangle \tag{11}$$

for the element $\mathcal{T}_{\beta\alpha}$ of the resonant-transition matrix. In a traditional interpretation the elements of this matrix give the amplitude of probability for the system to be found in a final scattering state β, provided it initially is prepared in the scattering state α. $\mathcal{T}^{\text{nonres}}_{\beta\alpha}(\varepsilon',\varepsilon,E)\equiv Y^{+}_{\beta\alpha}(\varepsilon',\varepsilon)$ gives the contribution of a pure resonant-scattering event. From $\mathcal{T}_{\beta\alpha}(\varepsilon',\varepsilon,E)$ we can extract useful information about the formation and the decay of the core-hole state, i.e., we can obtain the transition matrix for the photoionization and the x-ray or Auger emission processes. Let us consider this in more detail.

It has been understood that the process is free from PCI effects involving the primary photoelectron. One consequence of this is that the whole resonant-scattering event can be studied *as* if it occurs in two independent steps: the formation and the delayed decay of the intermediate (resonant) state.[24(f)] From this outset we derive an expression of the transition-matrix elements corresponding to the photoionization process by writing an element of the resonant contribution of the $\underline{\mathcal{T}}$ matrix as

$$\mathcal{T}^{\text{res}}_{\beta\alpha}(\varepsilon',\varepsilon,E)=\langle[\tilde{M}^{-}_{\beta}(\varepsilon',E)]^{\dagger}|\Upsilon^{+}_{\alpha E}(\mathbf{R})\rangle \ . \tag{12}$$

We observe that $\mathcal{T}^{\text{res}}_{\beta\alpha}(\varepsilon',\varepsilon,E)$ is formed as a scalar product between the ket $|\Upsilon^{+}_{\alpha E}(\mathbf{R})\rangle$ and the bra $\langle[\tilde{M}^{-}_{\beta}(\varepsilon',E)]^{\dagger}|$. The latter object clearly contains all information about the final channel β through $\Psi^{-}_{\beta\varepsilon'}(\mathbf{r},\mathbf{R})$. The coupling between the resonant state and the final channel is achieved through the operator $(\hat{H}-E)$ which also is included in the bra $\langle[\tilde{M}^{-}_{\beta}(\varepsilon',E)]^{\dagger}|$. Hence $\langle[\tilde{M}^{-}_{\beta}(\varepsilon',E)]^{\dagger}|$ contains all information about the decaying event with the exception, however, of the population of the vibrational levels in the intermediate state. These pieces of information are certainly in the ket $|\Upsilon^{+}_{E}(\mathbf{R})\rangle$.

Let $\xi_{Em}(\mathbf{R})$ be the complex, energy-dependent eigenfunctions of the optical operator $\tilde{H}_{\phi}(\varepsilon_{e_1})+\tilde{F}(E)$, $W_m(\varepsilon_{e_1},E)$ the corresponding eigenvalues, and m denoting vibrational quantum numbers. From these considerations we see that

$$t^{\text{phot}}_{\alpha m}(\varepsilon_{e_1},\varepsilon,E)=\langle\xi_{Em}(\mathbf{R})|\Upsilon^{+}_{\alpha E}(\mathbf{R})\rangle \tag{13}$$

is a proper element of the transition matrix for the excitation process. The cross section for the primary photoionization process is given by

$$\sigma^{\text{phot}}_{\alpha}(\varepsilon_{e_1})\propto\sum_{m}|t^{\text{phot}}_{\alpha m}(\varepsilon_{e_1},\varepsilon,E)|^2\,\delta(\mathcal{E}_{\alpha}+\hbar\omega-E) \tag{14}$$

which, when combined with Eqs. (13) and (9), leads to

$$\sigma^{\text{phot}}_{\alpha}(\varepsilon_{e_1})\propto\sum_{m}\left|\frac{\langle\xi_{Em}(\mathbf{R})\phi(\mathbf{r};\mathbf{R})|\hat{H}-E|\Psi^{+}_{\alpha}(\mathbf{r},\mathbf{R})\rangle}{E-\tilde{H}_{\phi}(\varepsilon_{e_1})-\tilde{\Delta}(E)+(i/2)\tilde{\Gamma}(E)}\right|^2$$

$$\times\delta(\mathcal{E}_{\alpha}+\hbar\omega-E) \ . \tag{15}$$

Returning to the study of the complete resonant-scattering event we note that the elements of the resonant-transition matrix of Eq. (11) can be factorized as

$$\mathcal{T}^{\text{res}}_{\beta\alpha}(\varepsilon',\varepsilon,E)=\sum_{n}t^{\text{decay}}_{\beta n}(\varepsilon',E)t^{\text{phot}}_{n\alpha}(\varepsilon_{e_1},\varepsilon,E) \ , \tag{16}$$

which explicitly shows the dependency of the transition matrix for the photoionization process, Eq. (13), and with

$$t^{\text{decay}}_{n\beta}(\varepsilon',E)=\langle[\tilde{M}^{-}_{\beta}(\varepsilon',E)]^{\dagger}|\xi_{En}(\mathbf{R})\rangle \ . \tag{17}$$

The cross section corresponding to the x-ray or Auger emission is then

$$\sigma_{\beta\alpha}^{\text{emiss}}(\varepsilon',\varepsilon,E)\propto\sum_{n_\beta}\left|\sum_n\langle\tilde{M}^-_\beta(\varepsilon',E)]^\dagger|\xi_{En}(\mathbf{R})\rangle\langle\xi_{En}(\mathbf{R})|\Upsilon^+_{\alpha E}(\mathbf{R})\rangle\right|^2\delta(\mathcal{E}_\beta+\varepsilon'-E)$$

$$\propto\sum_{n_\beta}\left|\sum_n\frac{\langle[\tilde{M}^-_\beta(\varepsilon',E)]^\dagger|\xi_{En}(\mathbf{R})\rangle\langle\xi_{En}(\mathbf{R})|\tilde{M}^+_\alpha(\varepsilon,E)\rangle}{E-W_n(\varepsilon_{e_1},E)}\right|^2\delta(\mathcal{E}_\beta+\varepsilon'-E)$$

$$\propto\sum_{n_\beta}\left|\sum_n\frac{\langle[\tilde{M}^-_\beta(\varepsilon',E)]^\dagger|\xi_{En}(\mathbf{R})\rangle\langle\xi_{En}(\mathbf{R})|\tilde{M}^+_\alpha(\varepsilon,E)\rangle}{E-\tilde{H}_\phi(\varepsilon_{e_1})-\tilde{\Delta}(E)+(i/2)\tilde{\Gamma}(E)}\right|^2\delta(\mathcal{E}_\beta+\varepsilon'-E)\ . \tag{18}$$

Previously, Gelmukhanov *et al.*,[11,12] Domcke *et al.*,[8] and Kaspar *et al.*[13] derived equations for molecular vibronic cross sections for photoionization and electronic decaying processes equivalent to Eqs. (15) and (18), respectively. Domcke and Kaspar solved iteratively the equation for the transition operator $\hat{T}$ in a space spanned by a direct product of an antisymmetrized product of orthonormalized (discrete and continuum) electronic one-particle states and a vibrational (harmonic oscillator) state using a model molecular Hamiltonian which incorporates a linear electron-nuclear coupling of motion through the so-called first-order coupling constant.[25]

In order to derive computable expressions from the photoionization, Auger, and x-ray emission cross sections, given above, we have to address the nuclear-motion problem posed by the nuclear Hamiltonians $\tilde{H}_\phi+\tilde{F}(E)$ of the intermediate state and $\tilde{H}_\gamma$ of the several scattering channels γ, including the initial one α. In this work we will treat the problem for general dimensionality of the motion, but we also confine ourselves to the harmonic oscillator approximation for all involved states. This has the advantage that we can derive closed analytical expressions for the final cross sections. The solution for the initial state nuclear motion is supposed to be known, having the dimensionless normal coordinate $\{\mathbf{q}_\alpha\}$. These coordinates are related to the normal coordinates $\{\mathbf{Q}_\alpha\}$ through $\mathbf{q}_\alpha\equiv(\underline{\omega}^{(\alpha)})^{1/2}\mathbf{Q}_\alpha$, where $\omega_{ij}^{(\alpha)}=\omega_i^{(\alpha)}\delta_{ij}$ are the harmonic frequencies associated to the ith normal mode of the initial electronic state α. The solution of the Schrödinger equation for this state is given by the well-known wave functions

$$\chi_\alpha(\mathbf{q}_\alpha)=\prod_i\left[\frac{1}{2^{n_i}n_i!\pi^{1/2}}\right]^{1/2}\mathcal{H}_{n_i}(q_{\alpha_i})e^{-q_{\alpha_i}^2/2} \tag{19}$$

with eigenvalues

$$\epsilon^{(\alpha)}_{n_1,n_2,\ldots}=\sum_i\omega_i^{(\alpha)}(n_i+\tfrac{1}{2})\ , \tag{20}$$

where $\mathcal{H}_{n_i}(q_{\alpha_i})$ are the Hermite polynomials. For the treatment of the nuclear motion of other ionic states we take an expansion of the nuclear BO potential energy $\mathcal{E}_\beta$ ($\beta\neq\alpha$) in a Taylor series, in terms of the dimensionless coordinates $\mathbf{q}_\alpha$, around the equilibrium geometry of the initial state α defined by $\mathbf{q}_\alpha=0$. Up to second order, the approximated Hamiltonian H_β reads

$$\tilde{H}_\beta=-\tfrac{1}{2}\sum_i\omega_i^{(\alpha)}\frac{\partial^2}{\partial q_{\alpha_i}^2}+\sqrt{2}\vec{\kappa}^{\mathrm{t}}\cdot\mathbf{q}_\alpha+\tfrac{1}{2}\mathbf{q}_\alpha^{\mathrm{t}}\underline{\omega}^{(\alpha)}\mathbf{q}_\alpha$$
$$+2\mathbf{q}_\alpha^{\mathrm{t}}\underline{\lambda}\mathbf{q}_\alpha+V_0^{(\beta\alpha)}\ , \tag{21}$$

where the column vector $\vec{\kappa}$, with elements

$$\kappa_i=\frac{1}{\sqrt{2}}\partial[\mathcal{E}_\beta(\mathbf{q}_\alpha)-\mathcal{E}_\alpha(\mathbf{q}_\alpha)]/\partial q_{\alpha_i}|_{\mathbf{q}_\alpha=0}\ ,$$

and the square matrix $\underline{\lambda}$, with elements

$$\lambda_{ij}=\tfrac{1}{4}\partial^2[\mathcal{E}_\beta(\mathbf{q}_\alpha)-\mathcal{E}_\alpha(\mathbf{q}_\alpha)]/\partial q_{\alpha_i}\partial q_{\alpha_j}|_{\mathbf{q}_\alpha=0}$$

are the first and second-order coupling constant, respectively, as defined by Cederbaum and Domcke[25] and

$$V_0^{(\beta\alpha)}=[\mathcal{E}_\beta(\mathbf{q}_\alpha)-\mathcal{E}_\alpha(\mathbf{q}_\alpha)]|_{\mathbf{q}_\alpha=0}\ .$$

This approximated nuclear Hamiltonian has been shown successful for producing vibronic profiles in different types of electronic spectra such as valence- and inner-shell photoelectron, Auger, x-ray emission, and electron-molecule resonant-scattering spectra.[8,26–28] Even when the true potentials have large anharmonic contributions this particular form of Hamiltonian has demonstrated both qualitative and quantitative power for predictions of vibronic band shapes.[26,29] One reason for this is that quadratic expansions of the potential energy surfaces give a reasonably accurate nuclear Hamiltonian provided the nuclei (in the excited state) execute small displacements around the center of the expansion $\mathbf{q}_\alpha=0$. Stated in a more precise way, whenever the final molecular geometry remains within the Franck-Condon zone for times long enough for an experimental measurement, then most probably the experimental outcome in the form of a spectrum will be an image of the dynamics of the molecular system only at the neighborhood of $\mathbf{q}_\alpha=0$, an indication that a theoretical account of the event may not demand information about the full potential energy surface (PES) but only about a local region of it. In other words, if the Hamiltonian of Eq. (21) is used, the short-time dynamics of the process is properly taken in account, and therefore the envelope of a vibronic band should agree with results of a more rigorous calculation but the finer details are poorly estimated. A demonstration of this statement is given in Ref. 25 in terms of analysis of the moments of a vibronic line shape or in Ref. 30 where a time-dependent description of vibronic transitions is adopted.

After the ionization has taken place, the nuclei are exposed to a new energy potential $\mathcal{E}_\beta$ different from $\mathcal{E}_\alpha$. It implies that the coordinates $\mathbf{q}_\alpha$ are no more the normal modes of the new energy surface $\mathcal{E}_\beta$ nor is $\underline{\omega}^{(\alpha)}$ its set of harmonic frequencies. Instead, still keeping the quadratic form of the Hamiltonian of Eq. (21), we can consider a new set of normal coordinates $\mathbf{q}_\beta$ related to $\mathbf{q}_\alpha$ through the linear transformation

$$\mathbf{q}_\beta = \underline{J}^{(\beta\alpha)}\mathbf{q}_\alpha + \vec{\sigma}^{(\beta\alpha)} . \tag{22}$$

Define

$$\begin{aligned} \underline{J}^{(\beta\alpha)} &= (\underline{\omega}^{(\beta)})^{1/2}\underline{L}_\beta^{-1}\underline{V}\,\underline{L}_\alpha(\underline{\omega}^{(\alpha)})^{-1/2}, \\ \vec{\sigma}^{(\beta\alpha)} &= \sqrt{2}\underline{\Omega}^{-1}(\underline{J}^{(\beta\alpha)-1})^{\mathrm{t}}\vec{\kappa} , \end{aligned} \tag{23}$$

where the matrices $\underline{V}$ and $\underline{\Omega}$ (the prediction of the excited-state harmonic frequencies) are determined by solving the matrix equations

$$\underline{G}_\beta = \underline{V}\,\underline{G}_\alpha\underline{V}^{\mathrm{t}} , \tag{24a}$$

$$\underline{\omega}^{(\alpha)} + 4\underline{\lambda} = \underline{J}^{(\beta\alpha)\mathrm{t}}\underline{\Omega}\,\underline{J}^{(\beta\alpha)} , \tag{24b}$$

and further, if the dependence of the kinematic matrix $\underline{G}$ on the nuclear coordinates is neglected, Eq. (21) then assumes the form

$$\begin{aligned} \tilde{H}_\beta = &-\tfrac{1}{2}\sum_i \omega_i^{(\beta)}\frac{\partial^2}{\partial q_{\beta_i}^2} + \frac{1}{2}\mathbf{q}_\beta^{\mathrm{t}}\underline{\Omega}\mathbf{q}_\beta \\ &-\vec{\kappa}^{\mathrm{t}}\underline{J}^{-1}\underline{\Omega}^{-1}(\underline{J}^{-1})^{\mathrm{t}}\vec{\kappa} + V_0^{(\beta\alpha)} . \end{aligned} \tag{25}$$

$\underline{L}$ and $\underline{G}$ are the Wilson transformation and kinematic matrices, respectively,[31] and we have required that the $\underline{L}$ transformation matrices are properly normalized towards the $\underline{G}$ matrices of the actual state, i.e., defining them as $\underline{G}_\alpha = \underline{L}_\alpha\underline{L}_\alpha^{\mathrm{t}}$ and $\underline{G}_\beta = \underline{L}_\beta\underline{L}_\beta^{\mathrm{t}}$. In general, $\underline{J}^{(\beta\alpha)}$ is not a symmetric matrix although the transformation of Eq. (22) [together with the condition of Eq. (24a)] does characterize an operation of rotation-translation in the normal-mode coordinate space $\{\mathbf{Q}_\alpha\}$.[32] The Hamiltonian of Eq. (25) is not the correct harmonic nuclear Hamiltonian for the electronic state β because the matrices $\underline{\omega}^{(\beta)}$ and $\underline{\Omega}$ are not identical. While $\underline{\omega}^{(\beta)}$ is related to the curvature of $\mathcal{E}_\beta$ around $\mathbf{q}_\beta = \mathbf{0}$, $\underline{\Omega}$ reflects the curvature of that potential surface around $\mathbf{q}_\alpha = \mathbf{0}$. It is inherent in the method, however, that $\mathbf{q}_\beta$ is the correct set of (dimensionless) normal coordinates associated to $\tilde{H}_\beta$ provided $\mathcal{E}_\beta(\mathbf{q}_\alpha)$ has an exact harmonic behavior within the radius $|\vec{\sigma}^{(\beta\alpha)}|$ of a hypersphere centered at $-\underline{J}^{(\beta\alpha)^{-1}}\vec{\sigma}^{(\beta\alpha)}$. Nevertheless, if we make the additional approximation of setting $\underline{\Omega} = \underline{\omega}^{(\beta)}$ we find

$$\begin{aligned} \tilde{H}_\beta = &-\tfrac{1}{2}\sum_i \omega_i^{(\beta)}\frac{\partial^2}{\partial q_{\beta_i}^2} + \tfrac{1}{2}\mathbf{q}_\beta^{\mathrm{t}}\underline{\omega}^{(\beta)}\mathbf{q}_\beta \\ &-\vec{\kappa}(\underline{J}^{\mathrm{t}}\underline{\omega}^{(\beta)}\underline{J})^{-1}\vec{\kappa} + V_0^{(\beta\alpha)} . \end{aligned} \tag{26}$$

The Hamiltonian of Eq. (26) is then the correct harmonic Hamiltonian for the nuclear motion of the molecular system in the electronic level β. The physical content of this Hamiltonian differs from that of Eq. (21) in that they focus on two different regions of the potential surface $\mathcal{E}_\beta$; around $\mathbf{q}_\alpha = \mathbf{0}$ for the Hamiltonian of Eq. (21), whereas around $\mathbf{q}_\beta = \mathbf{0}$ for the one of Eq. (26). It is interesting, however, to note that the predicted minimum of the $\mathcal{E}_\beta(\mathbf{q}_\alpha)$ surface does depend only on the ratio of its first- and second-order coupling constants (and the initial-state harmonic frequencies), i.e.,

$$\mathbf{q}_\alpha^{\min} = -\underline{J}^{(\beta\alpha)-1}\vec{\sigma}^{(\beta\alpha)} = -\sqrt{2}(\underline{\omega}^{(\alpha)} + 4\underline{\lambda})^{-1}\vec{\kappa} .$$

If $\mathbf{q}_\alpha^{\min}$ [roughly $(\underline{\omega}^{(\alpha)})^{-1}\vec{\kappa}$)] is found to be small, Eq. (28) is certainly a good (harmonic) approximation for the exact $\tilde{H}_\beta$ operator. However, the use of a closed form for the $\underline{J}^{(\beta\alpha)}$ matrix Eq. (23) and the suggested approximation of $\underline{\Omega}$ by $\underline{\omega}^{(\beta)}$ can seriously compromise the equivalence between Eqs. (21) and (26), since the condition in Eq. (24b) can no longer hold. The correct procedure would be to solve the system of equations (24) to determine $\underline{J}^{(\beta\alpha)}$ and $\underline{\Omega}$. However, in such a case we can simply ignore the second-order coupling constant in Eq. (21) and obtain an expression for $\tilde{H}_\beta$ like Eq. (26) with $\underline{\omega}^{(\beta)}$ and $\underline{J}^{(\beta\alpha)}$ replaced by $\underline{\omega}^{(\alpha)}$ and $\underline{1}$, respectively. It has been argued[26,29] that such a level of approximation does, indeed, include some anharmonic character of the $\mathcal{E}_\beta(\mathbf{q}_\alpha)$ surface near the vertical point $\mathbf{q}_\alpha = 0$, i.e., the region where the vibrational transition with strong intensities resides, while weaker bands at the flanks of the progressions are comparatively poorly reproduced. As a conclusion we can state that the form Eq. (26) is a good approximation for the Hamiltonian $\tilde{H}_\beta$ for the cases where $(\underline{\omega}^{(\alpha)})^{-1}\vec{\kappa}$ is small (≤ 1, say) whereas the simplified form Eq. (21) (with $\underline{\lambda} = \underline{0}$) constitutes a better approximation than Eq. (26) for larger values of $(\underline{\omega}^{(\alpha)})^{-1}\vec{\kappa}$. See Refs. 28 and 29 for some illustrations of these points.

The solution for Eq. (26) is straightforward; the wave functions are

$$\chi_\beta(\mathbf{q}_\beta) = \prod_i \left[\frac{1}{2^{n_i} n_i! \pi^{1/2}}\right]^{1/2} \mathcal{H}_{n_i}(q_{\beta_i}) e^{-q_{\beta_i}^2/2} \tag{27}$$

and the eigenvalues

$$\epsilon_{n_1,n_2,\ldots}^{(\beta)} = \sum_i \omega_i^{(\beta)}(n_i + \tfrac{1}{2} - \tfrac{1}{2}|\sigma_i^{(\beta\alpha)}|^2) + V_0^{(\beta\alpha)} . \tag{28}$$

The quantity

$$V_0^{(\beta\alpha)} - \textstyle\sum_i(\omega_i^{(\beta)}/2)|\sigma_i^{(\beta\alpha)}|^2$$

is readily identified as the difference between the minima of the two electronic energy surfaces.

An equivalent treatment for the intermediate state Hamiltonian operator $\tilde{H}_\phi(\varepsilon_{e_1}) + \tilde{F}(E)$ is not straightforward due its nonlocal character and the implicit energy dependence brought by the $\tilde{F}(E)$ operator. However, since we are here confining ourselves to analyze a limited spectral range of energy, more precisely the one corresponding to a few vibrational levels of the intermediate state, it is reasonable to expect that within this range of energy $\tilde{F}(E)$ is a slowly varying function of E. This al-

lows us to significantly reduce the complexity of the $\tilde{F}(E)$ operator just by removing its energy dependence. The use of a nonlocal versus local operator has been rather extensively discussed in connection with resonant-electron scattering, where the 2.3-eV resonance in N_2 is the prime example.[33] The ongoing improvement in energy resolution of x-ray and Auger emission spectra may, however, call for explicit construction of the nonlocality of $\tilde{F}$ to describe finer details in core-hole emission spectra. This nonlocality problem enters into $\tilde{F}$ through the projector $|\Psi^{-}_{\beta\epsilon'}(\mathbf{r},\mathbf{R})\rangle\langle\Psi^{-}_{\beta\epsilon'}(\mathbf{r},\mathbf{R})|$ incorporated in the product $\tilde{M}^{-}_{\beta}(\varepsilon',E)[\tilde{M}^{-}_{\beta}(\varepsilon',E)]^{\dagger}$ of Eq. (10). We see that vibronic (intra-)channel mixing and nonadiabatic corrections to the background subspace of wave functions [Eqs. (3) and (4)] together with the interchannel mixing and nonadiabatic corrections between the intermediate approximated wave function and those of the background [Eq. (10)] are the factors which confer the nonlocality to $\tilde{F}$. It should be noted that in spite of those factors, the function $\Psi^{\pm}_{\beta\epsilon'}(\mathbf{r},\mathbf{R})$ still can be factorized as $\tilde{\Psi}^{\pm}_{\beta\epsilon'}(\mathbf{r})\chi_{\beta}(\mathbf{R})$, the factor $\tilde{\Psi}^{\pm}_{\beta\epsilon'}$ is not a simple function of $\mathbf{R}$ but rather a complicated, nonlocal operator on the nuclear spatial coordinate space [see Eqs. (3) and (4)]. However, in a first-order approximation, we can obtain $\tilde{F}$ considering only the *electronic* intra- and interchannels mixing. To do this we refer to the closure relation for $|\chi_{\beta}(\mathbf{R})\rangle\langle\chi_{\beta}(\mathbf{R})|$ and ignore all terms where the nuclear kinetic energy operator $\hat{T}$ are involved in Eq. (4), then in Eq. (3), and finally in Eq. (10). At this level of approximation $\tilde{F}$ is transformed to a local function of $\mathbf{R}$ and takes the form

$$F(\mathbf{R})=\sum_{\beta}\lim_{\nu\to 0}\int d\varepsilon'\frac{|\langle\phi(\mathbf{r},\mathbf{R})|(\hat{H}-\hat{T})-E|\Psi^{-}_{\beta\epsilon'}(\mathbf{r};\mathbf{R})\rangle|^2}{[E-\mathcal{E}_{\beta}(\mathbf{R})-\varepsilon'+i\nu]}\,, \tag{29}$$

which is to be compared to the nonlocal expression of Eq. (10). $\Psi^{-}_{\beta\epsilon'}(\mathbf{r};\mathbf{R})$ is obtained by equations equivalent to Eqs. (3) and (4), where $\tilde{V}_{\beta\alpha}(\varepsilon',\varepsilon)$ now is replaced by $V_{\beta\alpha}(\varepsilon',\varepsilon;\mathbf{R})$ that only parametrically depends on the nuclear coordinate $\mathbf{R}$.

Even though we have approximated F as an energy-independent and (local) function of $\mathbf{R}$, the intermediate state is still described by a complex Hamiltonian. It implies that the first- and second-order coupling constants are complex and that we need to deal with a complex BO energy surface E_{β} and also complex frequencies $\underline{\Omega}$. The imaginary part of $\underline{\Omega}$ should be interpreted as a lifetime contribution from each individual vibrational level to the total lifetime Γ. This vibrational contribution is, however, expected to be much smaller compared to the electronic one, so with a good approximation we can take $\mathrm{Re}(\underline{\Omega})=\underline{\Omega}$. The above devised method resulting in Eqs. (21) and (26) will then holds also for the intermediate state.

Using the set of approximation worked out above and the zero-order outgoing and incoming wave functions, for the initial state α and for all alternatives final channels β, respectively, i.e., considering only the first term of the right side on Eq. (3), we obtain the following expressions for the cross sections (15) and (18), for photoionization and Auger or x-ray emission, respectively,

$$\sigma^{\mathrm{phot}}_{n_\alpha}(\varepsilon_{e_1})\propto\sum_{n}\frac{|\langle\xi_{En}(\mathbf{q})|\mathcal{M}_{\mathrm{el}}(\mathbf{q})|\chi_{n_\alpha}(\mathbf{q})\rangle|^2}{\left[\hbar\omega-\mathfrak{T}^{(\phi\alpha)}_{e}-\Delta(\mathbf{0})-\varepsilon_{e_1}+\sum_{i}[(\omega^{(\alpha)}_{i}n_{\alpha_i}-\omega^{(\phi)}_{i}n_i)-\frac{1}{2}\Delta\omega^{(\phi\alpha)}_{i}]\right]^2+\frac{1}{4}\Gamma^2(\mathbf{0})} \tag{30}$$

and

$$\sigma^{\mathrm{emiss}}_{\beta\alpha}(\varepsilon',\varepsilon,E)\propto\sum_{n_\beta}\left|\sum_{n}\frac{\langle\chi_{n_\beta}(\mathbf{q})|\mathcal{M}'_{\mathrm{el}}(\mathbf{q})|\xi_n(\mathbf{q})\rangle\langle\xi_n(\mathbf{q})|\mathcal{M}_{\mathrm{el}}(\mathbf{q})|\chi_{n_\alpha}(\mathbf{q})\rangle}{\left[\varepsilon'+\mathfrak{T}^{(\beta\phi)}_{e}-\Delta(\mathbf{0})+\sum_{i}[(\omega^{(\beta)}_{i}n_{\beta_i}-\omega^{(\phi)}_{i}n_i)+\frac{1}{2}\Delta\omega^{(\beta\phi)}_{i}]\right]+\frac{i}{2}\Gamma(\mathbf{0})}\right|^2. \tag{31}$$

The quantities $\mathcal{M}_{\mathrm{el}}(\mathbf{q})$ and $\mathcal{M}'_{\mathrm{el}}(\mathbf{q})$ correspond to the electronic transition moments, $\Delta(\mathbf{0})$ and $\Gamma(\mathbf{0})$ the energy shift and the lifetime evaluated at $\mathbf{q}_\alpha=\mathbf{0}$, respectively; and $\Delta\omega^{(\mu\nu)}_{i}=\omega^{(\mu)}_{i}-\omega^{(\nu)}_{i}$. In our treatment the decay takes place from the point on the intermediate potential energy surface where this state was populated in the primary photoionization process. The terms

$$\mathfrak{T}^{(\phi\alpha)}=V^{(\phi\alpha)}_{0}+\tfrac{1}{2}\omega^{(\phi)}_{i}|\sigma^{(\phi\alpha)}_{i}|^2$$

and

$$\mathfrak{T}^{(\beta\phi)}=V^{(\beta\phi)}_{0}+\tfrac{1}{2}\sum_{i}(\omega^{(\phi)}|\sigma^{(\phi\alpha)}_{i}|^2-\omega^{(\beta)}|\sigma^{(\beta\alpha)}_{i}|^2)$$

represent the predicted difference between the minima of the potential energy surfaces of the initial and intermediate states and the intermediate and final states, respectively. $V^{(\mu\nu)}_{0}=E^{(\mu)}(\mathbf{0})-E^{(\nu)}(\mathbf{0})$, as before, correspond to a vertical electronic energy difference between the states μ and ν evaluated at the equilibrium geometry of the initial molecular ground state, $\mathbf{q}_\alpha=0$.

The line profile for the decay processes, Eq. (31), differs from the pattern that would be formed by a superposition of a set of displaced Lorentzian shaped lines, characteristic for the ordinary ionization processes in molecules, Eq. (30). We find instead that the shape of bands that contain a number of final vibronic state n_β is given as a sum of direct and interference terms. The direct contributions are formed, for each n_α and n_β, as a set of Lorentzians bands

$$\sigma_{\beta\alpha}^{\mathrm{dir}}(n_\beta,n_\alpha;\varepsilon',\varepsilon,E)\propto\sum_n\frac{|\langle\chi_{n_\beta}(\mathbf{q})|\mathcal{M}'_{\mathrm{el}}(\mathbf{q})|\xi_n(\mathbf{q})\rangle\langle\xi_n(\mathbf{q})|\mathcal{M}_{\mathrm{el}}(\mathbf{q})|\chi_{n_\alpha}(\mathbf{q})\rangle|^2}{\left[\varepsilon'+\mathfrak{T}_e^{(\beta\phi(}-\Delta(\mathbf{0})+\sum_i[(\omega_i^{(\beta)}n_{\beta_i}-\omega_i^{(\phi)}n_i)+\tfrac{1}{2}\Delta\omega_i^{(\beta\phi)}]\right]^2+\tfrac{1}{4}\Gamma^2(\mathbf{0})} \tag{32}$$

corresponding to the sequential events of formation and decay of the nth vibrational level of the core-hole state. The interference contributions (cross terms) read

$$\sigma_{\beta\alpha}^{\mathrm{interf}}(n_\beta,n_\alpha;\varepsilon',\varepsilon,E)\propto\sum_n\sum_{m(\neq n)}\left[\frac{\langle\chi_{n\beta}(\mathbf{q})|\mathcal{M}'_{\mathrm{el}}(\mathbf{q})|\xi_n(\mathbf{q})\rangle\langle\xi_n(\mathbf{q})|\mathcal{M}_{\mathrm{el}}(\mathbf{q})|\chi_{n_\alpha}(\mathbf{q})\rangle}{\left[\varepsilon'+\mathfrak{T}_e^{(\beta\phi)}-\Delta(\mathbf{0})+\sum_i[(\omega_i^{(\beta)}n_{\beta_i}-\omega_i^{(\phi)}n_i)+\tfrac{1}{2}\Delta\omega_i^{(\beta\phi)}\right]+\frac{i}{2}\Gamma(\mathbf{0})}\right]$$
$$\times\left[\frac{\langle\chi_{n\beta}(\mathbf{q})|\mathcal{M}'_{\mathrm{el}}(\mathbf{q})|\xi_m(\mathbf{q})\rangle\langle\xi_m(\mathbf{q})|\mathcal{M}_{\mathrm{el}}(\mathbf{q})|\chi_{n_\alpha}(\mathbf{q})\rangle}{\left[\varepsilon'+\mathfrak{T}_e^{(\beta\phi)}-\Delta(\mathbf{0})+\sum_i[(\omega_i^{(\beta)}n_{\beta_i}-\omega_i^{(\phi)}m_i)+\tfrac{1}{2}\Delta\omega_i^{(\beta\phi)}]\right]+\frac{i}{2}\Gamma(\mathbf{0})}\right]^* \tag{33}$$

and correspond to second-order-like contributions for the combined process of formation and decay of the core-hole state where virtual vibrational transitions $n\leftrightarrow m$ $(m\neq n)$ are possible during the time (Γ^{-1}) of the existence of the intermediate state. Equation (33) has two interesting limiting cases which can be checked by inspecting the ratio

$$\gamma_{nm}=\left|\frac{\tau_n(n_\beta)-\tau_m(n_\beta)}{\Gamma(\mathbf{0})}\right|\quad(n\neq m)\,,$$

where

$$\tau_n(n_\beta)=\mathfrak{T}_e^{(\beta\phi)}(\mathbf{0})-\Delta(\mathbf{0})+\sum_i(\omega_i^{(\beta)}n_{\beta_i}-\omega_i^{(\phi)}n_i+\tfrac{1}{2}\Delta\omega_i^{(\beta\phi)})$$

is the transition energy between the vibronic levels n $[\equiv(n_1,n_2,\ldots)]$ of the core-hole ϕ and final β states, respectively. If $\gamma_{nm}\gg1$ for any choice of n and m $(n\neq m)$, the interference terms [Eq. (33)] do not appreciably contribute to the total cross section [Eq. (31)], and we expect well-defined Lorentzian-shaped peaks forming progressions associated to each individual vibrational level n_β of the final electronic state β. At the opposite extreme we have $\gamma_{nm}\ll1$, at least for an appropriate range of indices $m\neq n$. In this case, the intermediate state can be thought of as having a very short electronic lifetime, i.e., $\Gamma^{-1}(\mathbf{0})\ll1$, so that in the scattering event the intermediate vibrational fine structure cannot be discerned from a broad continuum background. Equation (31) can then be rewritten as

$$\sigma_{\beta\alpha}(n_\alpha,\bar{\varepsilon};\gamma\ll1)\propto\sum_{n_\beta}\frac{|\langle\xi_{n_\beta}(\mathbf{q})|\mathcal{M}'_{\mathrm{el}}(\mathbf{q})\mathcal{M}_{\mathrm{el}}(\mathbf{q})|\chi_{n_\alpha}(\mathbf{q})\rangle|^2}{\left[\bar{\varepsilon}-\left[\mathfrak{T}_e^{(\beta\alpha)}(\mathbf{0})+\sum_i(\omega_i^{(\beta)}n_{\beta_i}-\omega_i^{(\alpha)}n_{\alpha_i}+\tfrac{1}{2}\Delta\omega_i\right]\right]^2+\tfrac{1}{4}\Gamma(\mathbf{0})^2}\,, \tag{34}$$

where $\bar{\varepsilon}=\varepsilon-\varepsilon'$, $\varepsilon\approx\mathfrak{T}_e^{(\alpha\phi)}(\mathbf{0})$ showing that, in the $\gamma_{nm}\ll1$ regime, a single series of vibrational bands will be formed for each initial vibrational quantum numbers n_α. Close resemblance of this spectrum with the one corresponding to the electronic transition $\beta\leftarrow\alpha$, having a broad background due to the possibly large value of $\Gamma(\mathbf{0})$, should be observed.

We thus see that the interference terms, Eq. (33), contribute with decreasing degrees of importance for the evaluation of Eq. (31), as we pass from the $\gamma_{nm}\ll1$ to the $\gamma_{nm}\gg1$ regime. Of special interest are the cases where $\gamma_{nm}\approx1$. As a rule, provided that at least two vibrational levels are sufficiently populated in the intermediate state, the interference terms, Eq. (33), cannot be excluded from Eq. (31), and as a consequence, deformations in the shape of the bands of the direct spectrum should occur. These deformations can result in a displacement of the position of the intensity maximum of the electronic band and, even, drastically compromise spectroscopic analysis of emission spectra of molecular short-lived electronic states.[34]

III. COMPUTATION

From the analysis it is clear that a full *ab initio* construction of vibronic emission spectra from short-lived states requires knowledge about several quantities. Some of these are nontrivial to obtain *ab initio*. These quantities refer to equilibrium geometries, energy related parameters such as force fields, vibrational energies, vibronic coupling constants, normal coordinate transformation matrices, excitation and deexcitation electronic transition moments, i.e., photoelectron, x-ray, and Auger moments, nuclear variation of the electronic transition moments, core-hole state lifetimes and lifetime gradients, and discrete continuum-interaction energy shift and the nuclear variation of this shift. The intention of the present applications is to explore the relative importance of these quantities for the construction of the final x-ray and Auger emission band of water. Our goal is to employ reliable numerical values for these quantities, but we do not intend to discuss their calculation in any detail.

Equilibrium geometries and the energy-related quanti-

ties are obtained from multiconfiguration self-consistent field (MCSCF) calculations using many-centered Gaussian basis functions. These quantities are obtained in the present work for the ground and $1a_1$ core-hole state. All matrix elements, including the electrostatic interaction elements with the continuum functions (lifetime Γ and shift Δ) and their geometry dependencies are obtained from one-center, expanded basis sets including Slater and trigonometric functions. Calculations of the continuum functions were performed within the static-exchange approximation and the relevant cross sections were obtained by means of Stieltjes imaging. Except for the photoelectron and x-ray moments, which are obtained here, these quantities have been evaluated for water in our recent publications.[17–19] We refer to these publications for explanation of the methods and of computational details including checks on stability of results with respect to choice of basis sets. The photoelectron and x-ray moments were obtained within the sudden and dipole approximations using the same basis sets as for the other matrix elements, see Refs. 17 and 19, and using mutually nonorthogonal sets of orbitals for initial and final states. The MCSCF calculations were of complete active-space type using a basis set[35] that previously was employed[28] to calculate potential energy surfaces for some of the states included in this investigation. The choice of complete active space $(2-5a_1, 1-2b_1, 1-2b_2)$ was checked for a few states against combined MCSCF and multireference externally contracted configuration-interaction (CI)[36] calculations. We then did not find any significant variation of either the coupling constants or the vibronic spectra. The multidimensional nuclear integrals necessary to evaluate the intensities of the vibronic transitions were computed by using a modified Sharp and Rosenstock generating-function method.[37]

IV. RESULTS AND DISCUSSION

A. Excitation spectrum

The vibrational probability distribution of the intermediate core-hole state is given by the H_2O $(1a_1^{-1})$ photoionization spectrum and can be theoretically reproduced according to Eq. (30) in Sec. II. We have computed the quantities needed as input for an application of this equation, viz., the spectroscopic parameters referring to the ground and to the core-hole states, the first-order coupling constants, electronic transition moments and their dependence on the nuclear coordinates over a range of nuclear geometries around the ground-state equilibrium, lifetime width, and the energy shift. The results for these quantities are collected on the Tables I(a), II, III, and IV, respectively.

TABLE I. Geometrical parameters and first-order coupling constants $\vec{\kappa}$ for the ground neutral $X\,^1A_1$, core-hole $^2A_1(1a_1^{-1})$, and x-ray final states $\tilde{X}\,^2B_1(1b_1^{-1})$ and $\tilde{B}\,^2B_2(1b_2^{-1})$. R is the interatomic O—H separation and θ the H—O—H angle.

(a)

	$X\,^1A_1$		$^2A_1(1a_1^{-1})$	
	Theoretical[a]	Experimental[b]	Theoretical[a]	Theoretical[c]
R_{eq} (a.u.)	1.8207	1.8088	1.8274	1.790
θ_{eq} (deg)	105.3	104.52	119.0	122.4
ω_1 (eV)[f]	0.479	0.477	0.448	0.492
ω_2 (eV)[f]	0.209	0.205	0.166	0.176
$(f_{rr}+f_{rr'})$ (a.u.)	0.5406	0.536 61	0.4780	0.5837
$f_{r\theta}$ (a.u.)	0.0163	0.014 65	0.0028	0.0033
$f_{\theta\theta}$ (a.u.)	0.0509	0.048 89	0.0311	0.0350

(b)

	$\tilde{X}\,^2B_1$		$\tilde{B}\,^2B_2$
	Experimental[d]	Theoretical[e]	Theoretical[e]
R_{eq} (a.u.)	1.887 8	1.9037	2.1543
θ_{eq} (deg)	110.3	108.50	54.98
ω_1 (eV)[f]	0.402	0.420	0.329
ω_2 (eV)[f]	0.177	0.188	0.200
$(f_{rr}+f_{rr'})$ (a.u.)	0.380 9	0.421	0.2262
$f_{r\theta}$ (a.u.)		0.0093	0.0319
$f_{\theta\theta}$ (a.u.)	0.035 97	0.0410	0.0614

[a]Present results (see text).
[b]Reference 38.
[c]Reference 39.
[d]Reference 40.
[e]Reference 41.
[f]Indices 1 and 2 refer to the symmetric stretching and symmetric bending normal modes, respectively.

TABLE II. First-order coupling constants and vertical electronic transition energies (eV) evaluated at equilibrium geometry of the ground state of H_2O. Indices 1 and 2 as in Table I.

Ionic states	κ_1	κ_2	ΔE^{vert}	ΔE^{adiab}
		Core-hole		
$^2A_1(1a_1^{-1})$	−0.0264	−0.1224	539.649	539.580
		Final x-ray		
$\tilde{X}\,^2B_1(1b_1^{-1})$	−0.1970	−0.0492	11.796	12.615[a]
$\tilde{A}\,^2A_1(3a_1^{-1})$	−0.2090	−0.4582	13.995	13.839[a]
$\tilde{B}\,^2B_2(1b_2^{-1})$	−0.6252	0.5094	18.428	17.189[a]
		Final Auger		
$^1A_1(1b_1^{-2})$	−0.6866	−0.1180	39.64	
$^1B_1(1b_1^{-1}3a_1^{-1})$	−0.7658	−0.4983	41.41	
$^1A_1(3a_1^{-2})$	−0.8096	−0.8511	44.52	
$^1A_2(1b_1^{-1}1b_2^{-1})$	−1.1694	0.4137	45.06	
$^1B_2(3a_1^{-1}1b_2^{-1})$	−1.1884	0.0011	47.36	

[a]Taken from Ref. 40.

TABLE III. Linear dependence of photoelectron and x-ray transition moments $\mathcal{M}(q_1,q_2)=\mathcal{M}_0(1+a_1q_1+a_2q_2)$. q_1 and q_2 are the dimensionless stretching and bending normal coordinates.

Transition	$\mathcal{M}_0$ (a.u.)	a_1	a_2
$^2A_1(1a_1^{-1})\leftarrow\tilde{X}\,^1A_1$	0.876 6	-0.7195×10^{-2}	$-0.179\,17\times10^{-3}$
$\tilde{X}\,^2B_1\leftarrow{}^2A_1(1a_1^{-1})$	−0.063 5	-0.5394×10^{-2}	$0.960\,3\times10^{-4}$
$\tilde{A}\,^2A_1\leftarrow{}^2A_1(1a_1^{-1})$	−0.055 44	-0.5694×10^{-2}	0.040 8
$\tilde{B}\,^2B_2\leftarrow{}^2A_1(1a_1^{-1})$	0.054 9	−0.011 67	−0.012 87

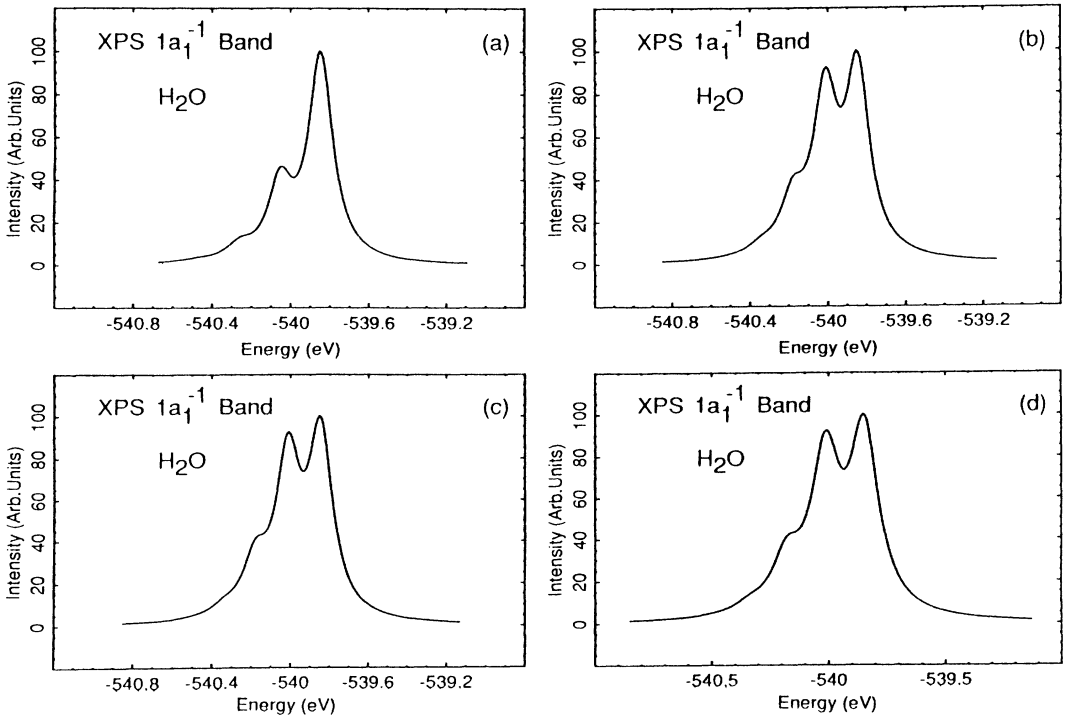

FIG. 1. $H_2O(1a_1^{-1})$ photoionization spectrum. (a) $FC1^0$, (b) FCJ^0, (c) NCJ^0, and (d) NCJ^G.

TABLE IV. Decay-rate function and energy shift for the core-hole state of water. All quantities are in units of eV and were evaluated at the neutral ground-state equilibrium geometry, $f(\mathbf{q})=f(\mathbf{0})+f_{q_1}q_1+f_{q_2}q_2$.

f	$f(\mathbf{0})$	$f_{q_1}(\mathbf{0})$	$f_{q_2}(\mathbf{0})$
$\Gamma(\mathbf{q})$[a,b]	0.15	-0.8722×10^{-3}	0.1308×10^{-2}
$\Delta(\mathbf{q})$[c]	0.06		

[a]Reference 17.
[b]Reference 18.
[c]Reference 19.

The simplest method we can employ to compute the photoionization spectrum, Eq. (30), is to adopt the Franck-Condon (FC) approximation for the vibronic transition, i.e., to assume the electronic moment transition $\mathcal{M}_{el}(\mathbf{q})$ constant over the normal coordinates, and to use the same force field for both initial ground and final core-hole electronic states. Next we introduce the complete transformation matrix $\underline{J}$. The non-Condon (NC) character of the transitions will be taken in account through a linear dependence of the electronic moment on the normal-mode coordinates. Finally the variation of lifetime with nuclear coordinates is considered. These levels of approximations are denoted FC1^0, FCJ^0, NCJ^0, and NCJ^G, respectively. In Table V we present the vibronic intensities for each of the cases described above. From this table we observe first that the $H_2O(1a_1^{-1})$ vibronic band essentially is formed by excitations of the bending normal mode with the (00←00) transition as the strongest one. The introduction of the complete matrix $\underline{J}$, Table VI, brings about some redistribution of the intensity for the lines belonging to different vibrational progressions. This is also reflected by the value of the (00←00) transition which experiences a reduction in intensity in favor of the higher ones. As we go to a linear non-Condon approximation—case NCJ^0—we observe that the strengths of the transitions (n_1n_2←00) do not differ much from that of the Franck-Condon FCJ^0 case. This is reflected by the relative small linear coefficients for the relevant electronic transition moments, shown in Table III.

The inclusion of the effect of a nonconstant linewidth is possible through calculation of the complex first-order coupling parameters with an imaginary part given by $1/(2\sqrt{2})\nabla_q[\Gamma(\mathbf{q})]_0$. Table IV shows the gradients $\partial\Gamma/\partial_{q_1}$ and $\partial\Gamma/\partial_{q_2}$ evaluated at the equilibrium geometry of the neutral initial state, $\mathbf{q}_{g.s.}=\mathbf{0}$. Except for the fundamental transition, the Franck-Condon amplitudes are now complex quantities. However, the introduction in our calculations of a nonconstant lifetime width does not imply any noticeable change of the values for the calculated Franck-Condon factors—compare the result for the cases NCJ^0 and NCJ^G. This result is also expected considering the smallness of the lifetime gradients compared to the (real) coupling constants. We thus have an example of an electronic transition where the validity of a constant resonance width approximation is quantitatively established.[18]

TABLE V. Strength of the symmetric stretch (n_1) and bend (n_2) vibrational transitions accompanying the $1a_1$ photoionization of water.

n_1	n_2	FC1^0	FCJ^0	NCJ^0	NCJ^G
0	0	0.6986	0.4586	0.4580	0.4580
0	1	0.2485	0.3907	0.3906	0.3906
0	2	0.0442	0.1273	0.1274	0.1274
0	3	0.0052	0.0184	0.0184	0.0184
0	4	0.0005	0.0009	0.0009	0.0009
1	0	0.0021	0.0027	0.0030	0.0030
1	1	0.0008	0.0009	0.0011	0.0011

TABLE VI. Normal-mode transformation matrix $\underline{J}$ is given along with the experimental force fields as used for the $X\,^1A_1$ ground and $\tilde{X}\,^2B_1$ ionic states and the theoretical force field for the $^2A_1(1a_1^{-1})$ and $\tilde{B}\,^2B_2$ ionic states (see Table I).

$$\begin{pmatrix} q_\beta^{(1)} \\ q_\beta^{(2)} \end{pmatrix} = \underline{J} \begin{pmatrix} q_\alpha^{(1)} \\ q_\alpha^{(2)} \end{pmatrix}$$

	$X\,^1A_1$
$^2A_1(1a_1^{-1})$	$\begin{bmatrix} 0.9675 & -0.0772 \\ 0.0243 & 0.8986 \end{bmatrix}$
$\tilde{X}\,^2B_1$	$\begin{bmatrix} 0.9391 & -0.0192 \\ 0.0070 & 0.9594 \end{bmatrix}$
$\tilde{B}\,^2B_2$	$\begin{bmatrix} 0.7768 & 0.4305 \\ -0.2330 & 0.9311 \end{bmatrix}$

Figures 1(a)–1(d) show the produced spectra for the four considered cases FC1^0, FCJ^0, NCJ^0, and NCJ^G, respectively. The FC1^0 and FCJ^0 cases have previously been investigated in Ref. 28, with results that compare quite well with the present ones.

As illustrated in Fig. 1, there are three bending quanta n_2 (=0,1,2) excited in the $H_2O(1a_1^{-1})$ photoionization process. The core-hole state has a predicted decay rate of 0.15 eV (Ref. 17) which is close to the differences of adjacent vibrational energy levels. We have, therefore, a good example of necessary conditions for the appearance of lifetime-vibrational interference effects in vibronic bands of core-hole emission. In the next subsections we study the H_2O decay spectra and derive the shape of some x-ray and Auger vibronic bands, paying special attention to interference effects in the vibrational structure. In all cases we shall, however, continue using the harmonic oscillator approximation for the nuclear-motion problem, which will be the main limitation in the experimental comparison. Since we are interested in comparing individual electronic bands only and not the full spectrum we use experimental adiabatic ionization energies for the intermediate and the final state to position the theoretical vibronic bands. For all calculations discussed below we find that the constant resonance width and crude adiabatic approximations are valid, and we do not comment on this further.

B. X-ray emission

The experimental x-ray emission spectrum of the $H_2O^+(1a^{-1})$ ion shows three main bands in the energy range of 520–530 eV (Ref. 42) [see Fig. 4(b)]. These

bands are assigned to electronic transitions leading to the creation of single valence-hole states, $\tilde{X}\,^2B_1$ (526.8 eV), $\tilde{A}\,^2A_1$ (525.1 eV), and $\tilde{B}\,^2B_1$ (520.4 eV) of the H_2O^+ ion. The observed line broadenings agree with the character of the nonbonding ($1b_1$), the angle bonding ($3a_1$), and the angle antibonding ($1b_2$) orbitals, respectively.

Figure 2 displays the computational results for the first x-ray band. Figure 2(a) was obtained by using a unit matrix as the normal coordinate transformation matrix $\underline{J}$ of the intermediate $1a_1^{-1}$ core-hole state, but keeping the complete matrix $\underline{J}$ relative to the $1b_1^{-1}$ final electronic state (thoughout this paper these matrices are constructed by using entries referring to the neutral ground and to a specified ionic state). The direct spectrum (dotted line) has four intensive transitions corresponding to (00←00), (01←00), (10←00), (11←00), and (20←00), from right to left. The inclusion of interference effects (dashed line) causes some changes on the band profile in the neighborhood of the main line. Briefly, it acts constructively near the position of the line (00←01) transition and at the left side of the main line, extending over the (01←00) transition, and destructively in the regions in between the position of the pairs of lines (00←01)-(00←00) and (01←00)-(10←00). The minor role played by the interference effects on the total line profile (curve in solid line) is mainly due to the lack of stronger excitations of the intermediate-state vibrational levels, when using a unit matrix $\underline{J}$ [see Fig. 1(a)]. The final shape of the x-ray band is derived by convoluting the theoretical spectra by a Gaussian function having a full width at half maximum (FWHM) of 0.35 eV, representing the instrumental spectrometer function.[42] The convoluted spectrum, the dashed-dotted curve in Fig. 2(a), shows a FWHM of ≈ 0.52 eV. The situation is somewhat changed when we introduce new transformation matrices $\underline{J}$ for the intermediate and the final $1b_1^{-1}$ states. Figures 2(b) and 2(c) show more realistic spectra produced by the use of the complete matrix $\underline{J}$ for the intermediate state and a unit matrix, Fig. 2(b), or the complete one, Fig. 2(c), for the final state. No noticeable differences can be seen comparing the curves in these two figures and, together with an analogous comparison between Figs. 1(a) and 1(b), we see that for the first x-ray band the inclusion of normal-mode mixing effect is far more important for the description of the intermediate state than for the final $1b_1^{-1}$ state. This conclusion is pefectly understandable if we inspect the respective matrices $\underline{J}$ for these two states, see Table VI. The large off-diagonal and the smaller (bending-mode) di-

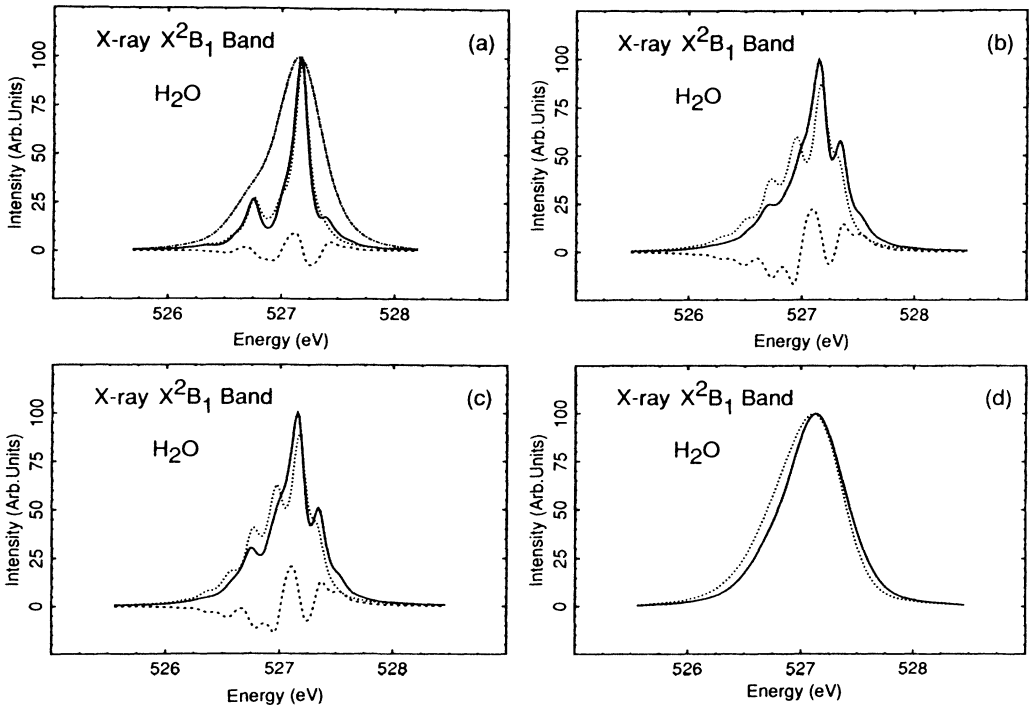

FIG. 2. First x-ray emission band of H_2O^+: $\tilde{X}\,^2B_1(1a_1^{-1}\leftarrow 1b_1)$. Results for different normal-mode transformation matrices for the intermediate $\underline{J}_{\rm int}$ and final $\underline{J}_f$ electronic states. (a) $\underline{J}_{\rm int}=\underline{J}_f=\underline{1}$, (b) full $\underline{J}_{\rm int}$ (see Table VI) and $\underline{J}_f=\underline{1}$, (c) full $\underline{J}_{\rm int}$ and $\underline{J}_f$ (see Table VI). In all cases, dashed, broken and solid lines correspond to the direct spectrum [Eq. (32)], interference spectrum [Eq. (33)] and the complete spectrum [Eq. (31)], respectively. (d) Corresponds to convolution of the Gaussian "instrumental" function (LWHM)=0.35 eV) with the direct (dotted line) and complete (solid line) spectra of (c). The curve with chain-dotted line in (a) is the Gaussian convolution (FWHM=0.35 eV) of the spectrum in full line.

agonal elements in the matrix $\underline{J}$ of the intermediate state are sufficient to account for the differences observed in Figs. 2(a) and 2(b) [or 1(a) and 1(b)] while the use of the matrix $\underline{J}$ close to unit for the $1b_1^{-1}$ state produces similar profiles for the spectra in Figs. 2(b) and 2(c). The direct contribution to Fig. 2(c) (dotted line) is formed by progressions of the bending mode in the final state rather than by the stretching progression as was the case in Fig. 2(a). Besides, the line corresponding to the first-harmonic (00←01) transition has gained intensity and is perfectly distinguished on the right side of the main line. The interference contributions (dashed line) have the same general qualitative behavior as before, but is now quantitatively stronger. The reason for this is that the strength of the interference effects is directly related to the degree of vibrational excitations in the intermediate state, which is stronger after the introduction of the complete matrix $\underline{J}$ [compare Figs. 1(a) and 1(b)]. These effects are responsible for the changes between Figs. 2(a) and 2(c). With the incorporation of the spectrometer broadening of 0.35 eV we obtain the spectra shown in Fig. 2(d). The interference affects the final band profile (solid line) by slightly shifting its maximum towards higher energies and reducing its FWHM by ≈ 0.7 eV with respect to the direct spectrum. The computed FWHM amounts to 0.64 eV.

The second band of the x-ray emission spectrum (525.1 eV), corresponding to the linear valence $\tilde{A}\,^2A_1$ state, was computed exploring the use of a unit and a nonunit matrix $\underline{J}$ for the intermediate state and a unit matrix for the final ionic state. The particular choice of a unit final-state matrix $\underline{J}$ was motivated by the relatively large value of the ratio $\kappa_2/\omega_2^{(\alpha)}$ which indicates that such a transformation matrix should better characterize the $\tilde{A}\,^2A_1$ state, according to the discussion in Sec. II. Actually, the corresponding band of the photoionization spectrum, which shows a single progression in the n_2 bending normal mode and strong anharmonicity of the potential energy surface along this coordinate,[40,43,44] is quite well reproduced if we employ the first-order coupling constants (see Table II) and a unit matrix $\underline{J}$,[45] [see Fig. 5(b)]. Figures 3(a) and 3(b) display the results for the second band of the x-ray spectrum considering these two cases discussed above. It is observed that the band shows a progression in the n_2 mode, quite equivalent to that of the photoelectron $(3a_1^{-1})$ band[40,43,44] [see Fig. 5(b)] having the intensity maximum for the peaks $n=6,7$. Again, the interference effects are stronger when mixing of the normal modes of the intermediate state are introduced, Fig. 3(b), although we see that they already have considerable strength even in the absence of the normal-mode mixing, Fig. 3(a). For both cases, the interference causes a reduction in the intensity of the peaks with n_2 lower than 7, while the opposite holds for the peaks with n_2 larger than 7. The consequence of this effect is apparent-

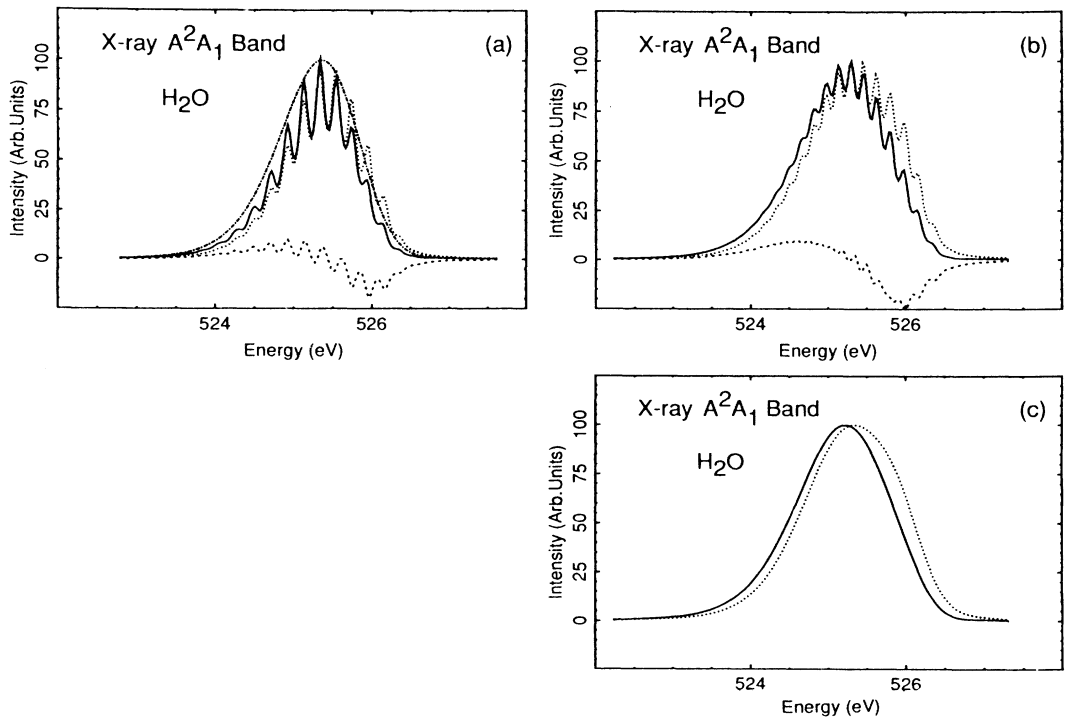

FIG. 3. Second x-ray emission band of H_2O^+: $\tilde{A}\,^2A_1;(1a_1^{-1}\leftarrow 3a_1)$. (a) $\underline{J}_{\rm int}=\underline{J}_f=\underline{1}$, (b) full $\underline{J}_{\rm int}$ (see Table VI) and $\underline{J}_f=\underline{1}$, (c) as Fig. 2(d). The dotted, broken, solid, and chain-dotted [(a)] lines as for Fig. 2.

ly a shift of ≈ 0.13 eV towards the lower energies and narrowing of the width by ≈ 0.09 eV. The general shape of the band, however, is maintained. The convoluted spectra are shown in the Fig. 3(c). The curve with solid line, which includes interference, has a FWHM of 1.45 eV.

As was the case for the second $3a_1^{-1}$ band, the theoretical analysis of the third x-ray band can be carried out considering only a unit matrix $\underline{J}$ for the $\tilde{B}\,^2B_2$ state. The first-order coupling constants for this state are presented in Table II. Their relatively large values imply a large normal-mode-shift vector, $\vec{\sigma}$ [Eq. (23)], and, consequently, strong excitations for both n_1 (stretching) and n_2 (bending) normal modes accompanying the electronic transition. By using unit or complete matrices $\underline{J}$ for the intermediate $1a_1^{-1}$ electronic state, we obtain the results displayed in Figs. 4(a) and 4(b), respectively. As manifested in the two previous cases, the introduction of a more realistic matrix $\underline{J}$ for the intermediate state results in an increase of intensity for the progression formed by transitions from the n_2 mode in the intermediate state and, also, its combination bands. The interference effects (dashed lines) reduce the intensity of the lines lying on the lower-energy part of the vibronic band, while the opposite holds for the high-energy region. The convoluted curves of Fig. 4(b) are shown in Fig. 4(c). We see that the interference narrows the FWHM of the band in dotted lines by ≈ 0.3 eV, shifts the band towards higher energies by about 0.7 eV and breaks its apparent symmetric shape. The FWHM of the final band (solid line) is 2.8 eV.

Although the results for the two first bands (widths, relative shifts, and shapes) can be considered quantitatively correct, the same cannot be said about the third band. The first-order coupling constant of the $\tilde{B}\,^2B_2$ ionic state can only roughly reproduce the corresponding third band of the experimental H_2O photoelectron spectrum,[40,43,44] see Fig. 5(c) and Ref. 45. The partial failure verified for the $\tilde{B}\,^2B_2$ band analysis may be attributed to the crossing between the potential energy surfaces of the $\tilde{B}\,^2B_2$ and $\tilde{A}\,^2A_1$ ionic states at the angle of $\approx 72°$.[46] Since the nuclear Hamiltonians we are dealing with are individually defined for each electronic potential energy

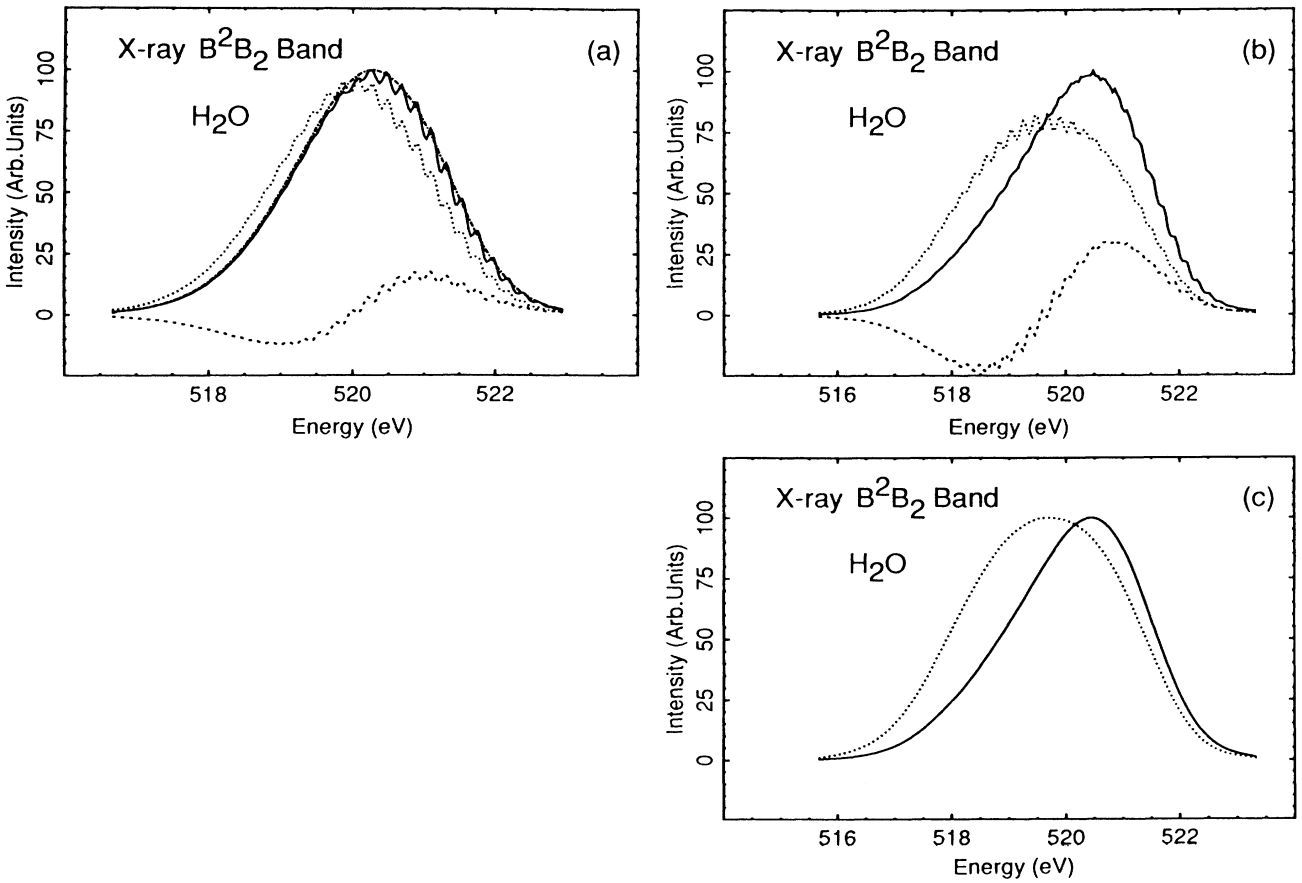

FIG. 4. Third x-ray emission band of H_2O^+: $\tilde{B}\,^2B_2(1a_1^{-1} \leftarrow 1b_2)$. (a) $\underline{J}_{\text{int}} = \underline{J}_f = \underline{1}$, (b) full $\underline{J}_{\text{int}}$ (see Table VI) and $\underline{J}_f = \underline{1}$, (c) as Fig. 2(d). The dotted, broken, solid, and chain-dotted [(a)] lines as for Fig. 2.

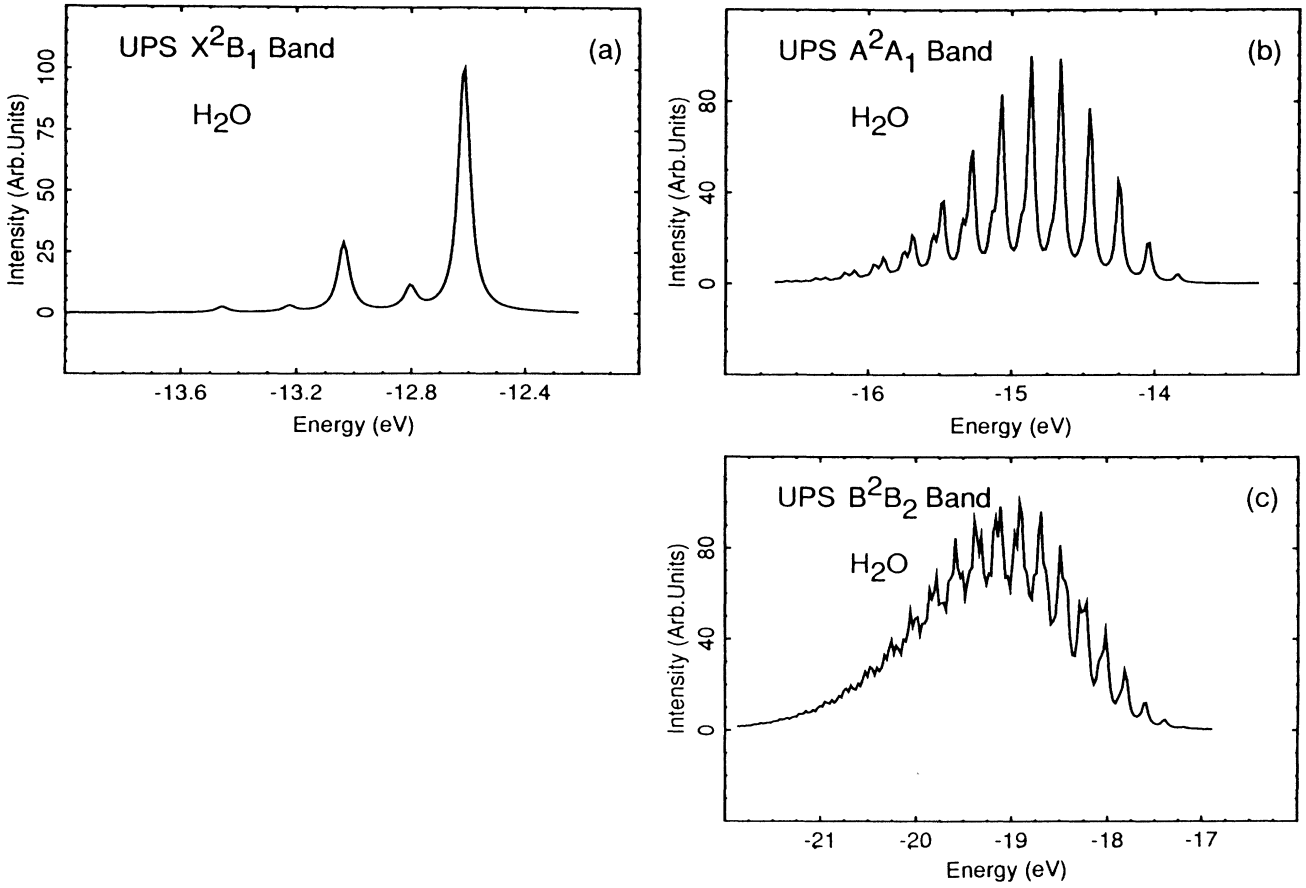

FIG. 5. Computed photoionization spectrum of H_2O. (a) $\tilde{X}\,^2B_1 \leftarrow X\,^1A_1$, first band; (b) $\tilde{A}\,^2A_1 \leftarrow X\,^2A_1$, second band; (c) $\tilde{B}\,^2B_2 \leftarrow X\,^1A_1$, third band.

surface, nothing regarding the perturbations due to curve crossings and/or the presence of near-lying electronic state(s) are inherent in our results. Therefore, we believe that the $\tilde{B}\,^2B_2$ photoelectron and its corresponding x-ray emission bands suffer from the shortcoming of the Born-Oppenheimer separation of the nuclear Hamiltonian in our calculations.

Finally, Figure 6(a) presents the calculated $H_2O(1a_1^{-1})$ x-ray vibronic spectrum in the energy region of 515.5–528.5 eV, including the three main bands. The bands of the direct spectrum (dotted line) was positioned by computing its corresponding adiabatic transition energy as a difference between the adiabatic ionization potential of the intermediate and final electronic states, see Table II. The relative intensity of these bands was taken from the experimental spectrum,[42] Fig. 6(b). The overall agreement of the computed and the experimental spectral profile is good. We observe that the effects of the vibrational-lifetime interference is of some importance for the experimental determination of adiabatic and/or vertical transition energies due to the apparent shifts caused for the vibronic bands. This is even more so for a detailed vibrational analysis because of the suppression, creation, or distortion of the fine structure in the vibronic bands. Certainly, a real test of the predicted vibrational spectrum needs better resolved experimental bands.

C. Auger emission

The Auger spectrum of water shows two main structures in the energy region between 490 and 500 eV.[47,48] The experimental spectrum is shown in Fig. 7 together with a theoretical spectrum obtained by our recently devised Stieltjes imaging technique for Auger spectra.[17] The experimental structures originate from the contributions of five electronic transitions that leave the molecule in double-ionized singlet states $^1A_1(1b_1^{-2})$, $^1B_1(3a_1^{-1}1b_1^{-1})$, $^1A_1(3a_1^{-2})$, $^1A_2(1b_2^{-1}1b_1^{-1})$, and $^1B_1(3b_2^{-1}3a_1^{-1})$. We have chosen these singlet states to illustrate the role of the vibrational interference in Auger emission.

The first-order coupling parameters for all of these states, shown in Table II, suggest that it is possible to obtain fairly good vibronic profiles if we only use unit normal-mode transformation matrices $\underline{J}$ for all final states. As the use of full matrices $\underline{J}$ already has been discussed in detail for x-ray emission, no attempt will be

made towards a more accurate description of the vibronic bands regarding the definite vibrational line positions and changes that might be introduced by the normal-mode-mixing effects.

Figures 8–10 show the bands corresponding to the transitions leading to the final ionic states $^1A_1(1b_1^{-2})$, $^1B_1$, and $^1A_2$, respectively. Using a one-particle language, we consider these three states as formed by a

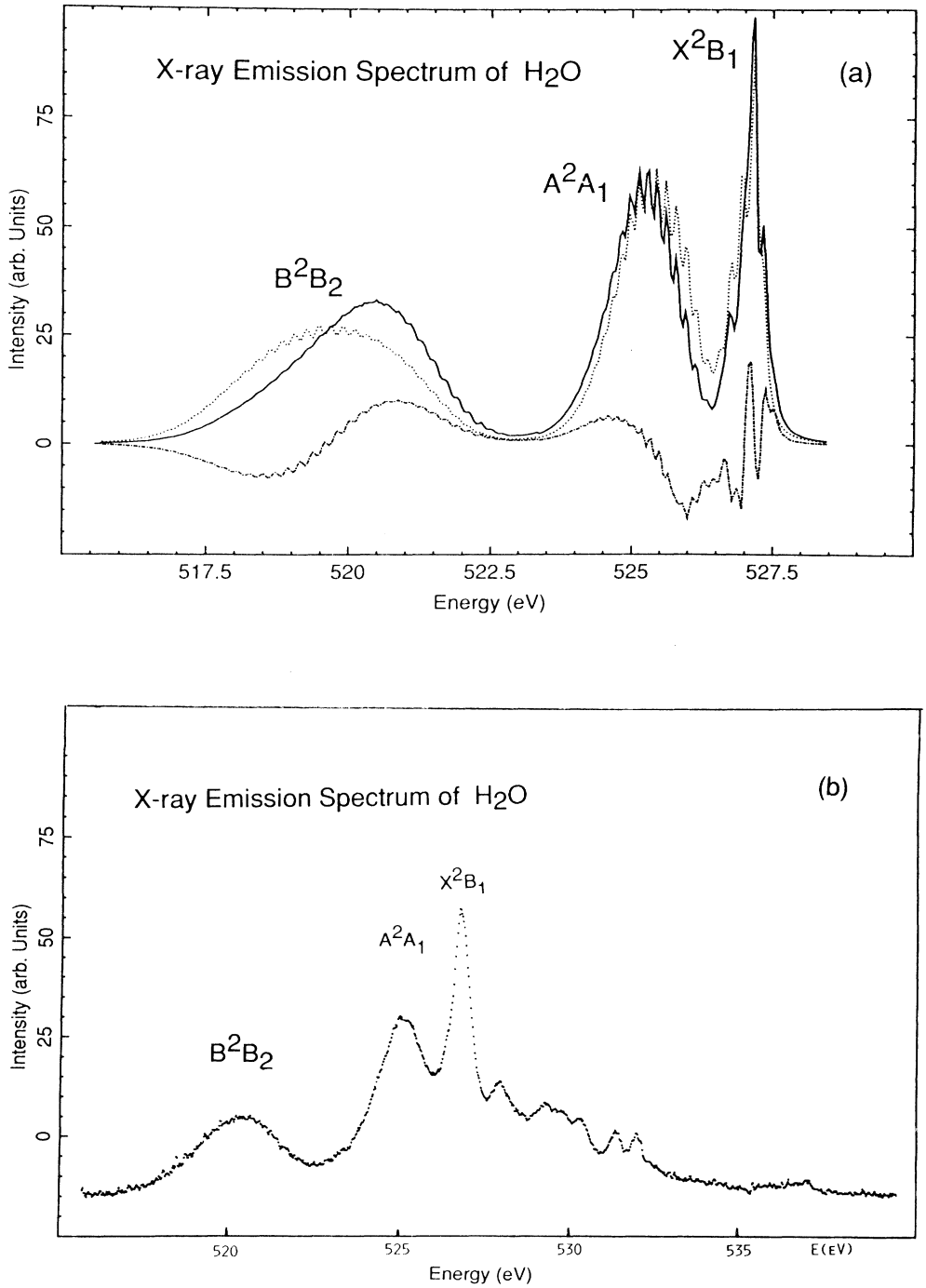

FIG. 6. $H_2O^+(1a_1^{-1})$ x-ray spectrum showing the three main bands $\tilde{X}\,^2B_1$, $\tilde{A}\,^2A_1$, $\tilde{B}\,^2B_2$, from right to left. (a) Calculated spectra and (b) experimental (Ref. 42).

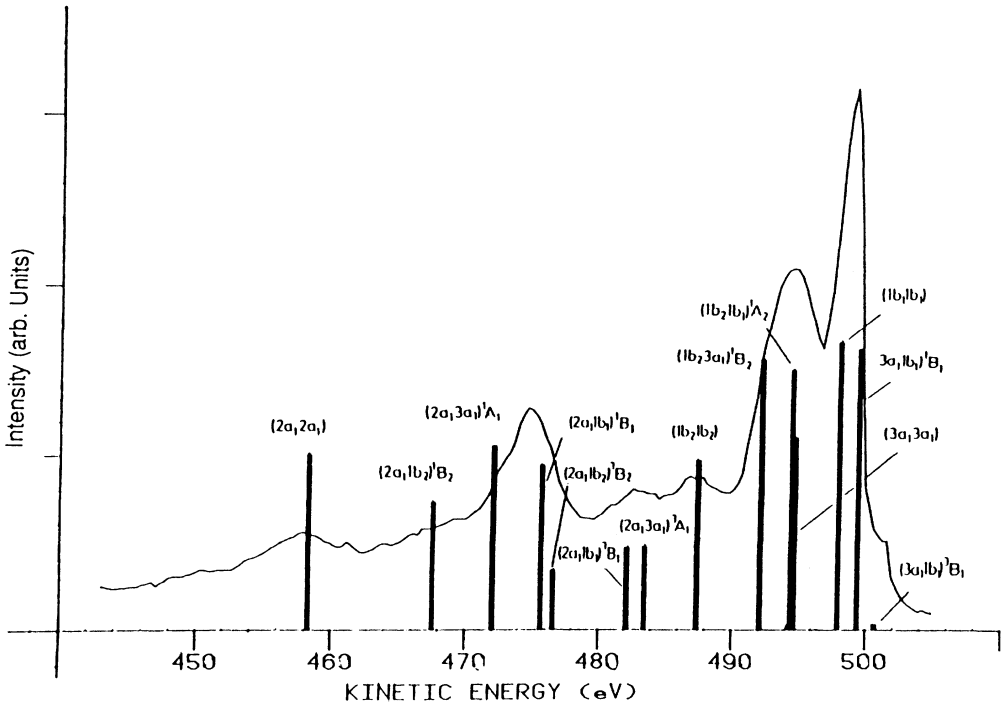

FIG. 7. $H_2O^+(1a_1^{-1})$ experimental Auger spectrum (Ref. 48). The bars represent resutls from calculations in Ref. 17.

removal of an extra nonbonding $1b_1$ orbital from each of the three x-ray final states, $\tilde{X}\,^2B_1$, $\tilde{A}\,^2A_1$, and $\tilde{B}\,^2B_2$, respectively. We observe from Table II that combinations of the single-ionic (x-ray emission) κ_2 coupling constants predict the corresponding double-ionic (Auger emission) coupling constants rather well. This, however, does not hold for the κ_1 constants, which may be an indication of a larger correlation (or differential correlation) effects for evaluating the stretching coupling constants. Further towards the low-kinetic energy side we expect, however, a complete failure of such combination rules due to the importance of the static-correlation effects. The Auger $^1B_1$

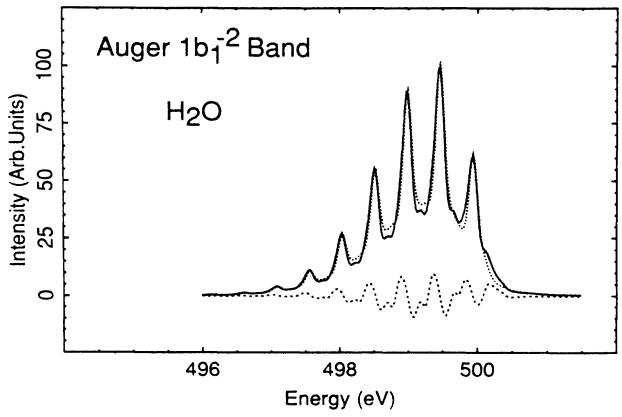

FIG. 8. $H_2O^{+2}(1b_1^{-2})\leftarrow H_2O^+(1a_1^{-1})$ Auger emission band. Full $\underline{J}_{\text{int}}$ (see Table VI) and $\underline{J}_f=\underline{1}$; the dotted, broken, and solid lines as in Fig. 2.

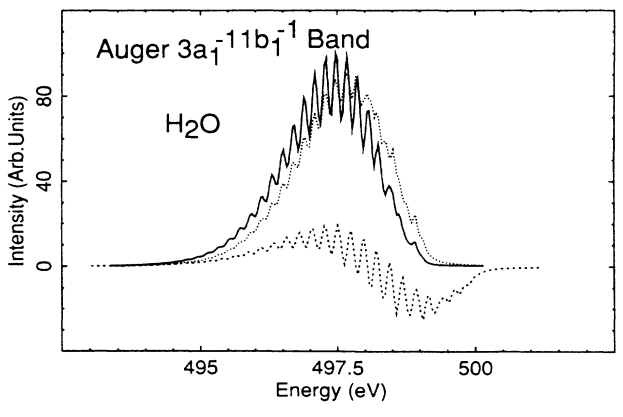

FIG. 9. $H_2O^{+2}(3a_1^{-1}1b_1^{-1})\leftarrow H_2O^+(1a_1^{-1})$ Auger emission band. Full $\underline{J}_{\text{int}}$ (see Table VI) and $\underline{J}_f=\underline{1}$; the dotted, broken, and solid lines as in Fig. 2.

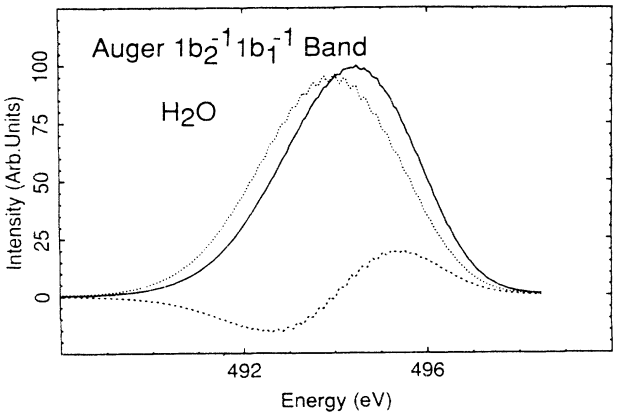

FIG. 10. $H_2O^{+2}(1b_2^{-1}1b_1^{-1})\leftarrow H_2O^{+}(1a_1^{-1})$ Auger emission band. Full $\underline{J}_{\rm int}$ (see Table VI) and $\underline{J}_f=\underline{1}$; the dotted, broken, and solid lines as in Fig. 2.

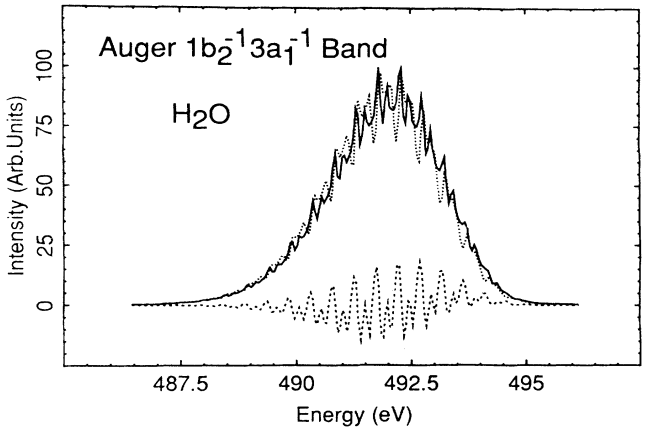

FIG. 12. $H_2O^{+2}(1b_2^{-1}3a_1^{-1})\leftarrow H_2O^{+}(1a_1^{-1})$ Auger emission band. Full $\underline{J}_{\rm int}$ (see Table VI) and $\underline{J}_f=\underline{1}$; the dotted, broken, and solid lines as in Fig. 2.

band, Fig. 9, and $^1A_2$ and, Fig. 10, resemble to some extent their x-ray counterparts, Figs. 3(b) and 4(b), respectively, showing similar vibrational progressions and interference patterns. On the other hand, the Auger $^1A_1(1b_1^{-1})$ and the x-ray $\tilde{X}\,^2B_1(1b_1^{-1})$ bands differ considerably from each other with respect to the number of excited n_1 stretching levels, a direct consequence of the large value of κ_1 for the former state. The n_2 bending progressions are completely hidden by the stronger n_1 progression although we still observe an interference contribution (dashed line) that almost periodically shows the pattern present in Fig. 2(b). The Auger bands corresponding to the formation of the $^1A_1(3a_1^{-2})$, Fig. 11, and $^1B_2$, Fig. 12, ionic states are both considerably excited in the n_1 mode, but they show different levels of excitations with respect to the n_2 mode. It is observed that the interference effects for the $^1A_1(3a_1^{-2})$ state show the same general behavior as for the Auger $^1B_2$ and x-ray $\tilde{A}\,^2A_1$

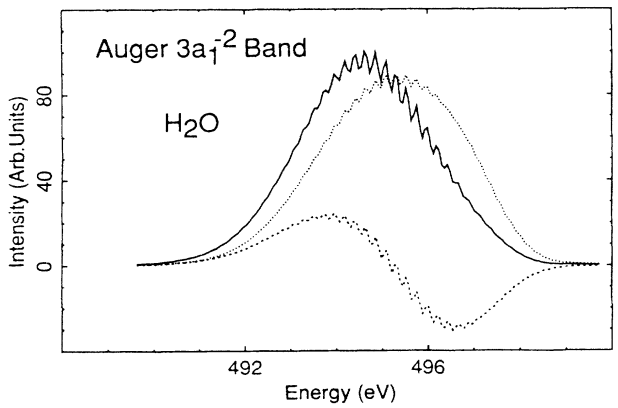

FIG. 11. $H_2O^{+2}(3a_1^{-2})\leftarrow H_2O^{+}(1a_1^{-1})$ Auger emission band. Full $\underline{J}_{\rm int}$ (see Table VI) and $\underline{J}_f=\underline{1}$; the dotted, broken, and solid lines as in Fig. 2.

cases, i.e., constructive character on the low-energy side of the vibronic band and destructive on its high-energy side, giving an apparent shift to the band towards the lower-energy region.

As a final remark, we observe that the five studied Auger bands have their calculated vertical ionization potential separated by about 2–3 eV, except the $^1A_1(3a_1^{-2})$ and $^1A_2$ ones which lie only $\sim$0.1 eV from each other.[17] In accordance with analysis of the x-ray $\tilde{B}\,^2B_2$ band in the previous section, we expect that the present results for the Auger bands have only a semiquantitative quality since the density of states probably calls for a solution of an improved nuclear Hamiltonian where nonadiabatic corrections are explicitly taken into account.

V. CONCLUSIONS

The first aim with the present work was to derive vibronic cross sections for x-ray and Auger decay from short-lived core-holes states in molecules starting from the Åberg's description of atomic x-ray and Auger decay as multichannel-scattering processes. The derivation includes a scattering-matrix formalism in which the intra- and interchannel interactions as well as nonadiabatic corrections are introduced. Computable expressions for x-ray and Auger emission are derived assuming the harmonic approximation for the nuclear motion.

We find that the vibrational profile of a decay spectrum from a short-lived state depends on several spectroscopic parameters and other quantities related to the states involved in the transitions. These refer to force fields, equilibrium geometries, variation of electronic moments with geometry, lifetime and discrete continuum-interaction energies and their geometry variation. A second aim with the present work was to demonstrate by means of a few numerical applications the relative importance of all these quantities in the construction of multidimensional vibronic x-ray and Auger spectra. Truly *ab initio* and reliable values have been calculated and used for all quantities involved.

We find for all the studied cases a negligible influence on the spectra from lifetime-nuclear variation (constant resonance width approximation holds), from nuclear variation of electronic moments (crude adiabatic approximation holds), and from the discrete continuum-interaction energy shift. However, for all cases we find considerable influence from lifetime-vibrational interference. In fact the present results indicate that for multidimensional vibronic spectra there can be substantial lifetime-vibrational interference even when the intermediate core-hole states are only moderately excited vibrationally.

We have also explored the role of different approximations in the treatment of the nuclear motion. All these approximation levels are confined to the harmonic approximation. This gives the possibility to derive fully analytical expressions including the lifetime parameters for all approximation levels. These levels refer to the use of vibronic coupling constants, diagonal force fields, and full (nonorthogonal) transformations between the sets of normal coordinates. The constructed vibronic profiles are found rather dependent on the choice of these approximation levels and so are also the finer details of the lifetime-vibrational interference. When there are considerable vibrational excitations, i.e., situations where the harmonic approximation is limited, the use of first-order vibronic constants seemingly gives better results than the full normal-mode transformation matrices. The latter give the exact cross sections in the harmonic case, but may greatly exaggerate combination bands otherwise. This observation is also in line with the analysis of Domcke and Cederbaum,[26,29] who showed that some degree of anharmonicity is accounted for when calculating vibronic intensities by first-order coupling constants. Finally, we find one case in the x-ray emission spectrum where our Born-Oppenheimer based analysis breaks down. We believe that this is a more common situation for Auger spectra due to the comparatively high density of molecular two-hole states.

ACKNOWLEDGMENTS

One of us (A.C.) would like to thank Professor Osvaldo Goscinski for helpful and instructive discussions. We thank Jan-Erik Rubensson and the x-ray emission group in Uppsala for making the original x-ray spectrum of water available to us and Joseph Nordgren, Svante Svensson, and Leif Karlsson for valuable discussion on x-ray and Auger spectroscopy. One of us (A.C.) acknowledges financial support of Conselho Nacional de Desenvolvimento Científico e Tecnológico (CNPq) (Brazil). This work was supported by the Swedish (H.Å.) and Italian Natural Science Research Councils, NFR and CNR.

[1]T. Åberg, Phys. Scr. **21**, 495 (1980); T. Åberg, and G. Howat, in *Encyclopedia of Physics*, edited by S. Flügge and W. Mehlhorn (Springer, Berlin, 1982), Vol. 31, p. 469.

[2]U. Fano, Phys. Rev. **124**, 1866 (1961).

[3]H. Feshbach, Ann. Phys. (N.Y.) **19**, 287 (1962).

[4]N. F. Lane, Rev. Mod. Phys. **52**, 29 (1980); M. A. Morrison, Aust. J. Phys. **36**, 239 (1983); A. K. Kazanskiĭ and I. I. Fabrikant, Usp. Fiz. Nauk **143**, 601 (1984) [Sov. Phys.—Usp. **27**, 607 (1984)].

[5]A. Herzenberg, J. Phys. B **1**, 548 (1968); D. T. Birtwistle and A. Herzenberg, *ibid* **4**, 53 (1971).

[6]J. C. Y. Chen, J. Chem. Phys. **40**, 3507 (1964).

[7]T. F. O'Malley, Phys. Rev. **150**, 14 (1966).

[8]W. Domcke and L. S. Cederbaum, Phys. Rev. A **16**, 1465 (1977).

[9]J. N. Bardsley, J. Phys. **1**, 349 (1968).

[10]F. H. Mies, Phys. Rev. **175**, 164 (1968).

[11]F. K. Gel'mukhanov, L. N. Mazalov, and N. A. Shklyaeva, Zh. Eksp. Teor. Fiz. **69**, 1971 (1975).

[12]F. K. Gel'mukhanov, L. N. Mazalov, A. V. Nikolaev, A. V. Kondratenko, V. G. Smirnii, P. I. Wadash, and A. P. Sadovskii, Dokl. Akad. Nauk SSSR **225**, 597 (1975); F. K. Gel'mukhanov, L. N. Mazalov, and A. V. Kondratenko, Chem. Phys. Lett. **46**, 133 (1977).

[13]F. Kaspar, W. Domcke, and L. S. Cederbaum, Chem. Phys. **44**, 33 (1979).

[14]N. Correia, A. Flores-Riveros, H. Ågren, K. Helenelund, L. Asplund, and U. Gelius, J. Chem. Phys. **83**, 2035 (1985); A. Flores-Riveros, N. Correia, H. Ågren, L. Pettersson, M. Bäckström, and J. Nordgren, *ibid.* **83**, 2053 (1985); Errata (to be published). Computational errors in these papers have been corrected by T. X. Carroll and T. D. Thomas, J. Chem. Phys. **86**, 5521 (1987).

[15]L. Ungier and T. A. Thomas, J. Chem. Phys. **82**, 3146 (1985); T. X. Carroll, S. E. Anderson, L. Ungier, and T. D. Thomas, Phys. Rev. Lett. **58**, 867 (1987); T. X. Carroll and T. D. Thomas, J. Chem. Phys. **86**, 5221 (1987); **89**, 5983 (1988).

[16]R. Murphy, Z.-W. Lyo and W. L. Eberhardt, J. Chem. Phys. **88**, 6078 (1988).

[17]V. Carravetta and H. Ågren, Phys. Rev. A **35**, 1022 (1987).

[18]H. Ågren, A. Cesar, and V. Carravetta, Chem. Phys. Lett. **139**, 145 (1987).

[19]V. Carravetta, H. Ågren, and A. Cesar, Chem. Phys. Lett. **148**, 210 (1988).

[20]Postcollision interaction accounts for the correlation between the two escaping particles through a coupling with the common residual ion (Ref. 24). PCI affects the line profile of a scattering process, such as the emitted Auger electron (strong effect) or x-ray photon emission (weak effect), shifting its maximum to higher energy and distorting it from the expected symmetrical Lorentzian profile. In the photoelectron spectrum the PCI effect changes the spectral line shape the opposite way. On classical grounds, this effect is caused by an exchange in energy between the two escaping particles due to the change in the electric field felt by the slow (i.e., small excess of energy ε_{e_1}) primary photoelectron when exposed to a different ionic environment after that the Auger (or x-ray) decay takes place. The theoretical treatments of this effect in atoms have been offered by semiclassical approximations [Refs. 24(b) and 24(c)], diagrammatic many-body perturbation [Ref. 24(d)] resonant scattering [Refs. 1 and 24(e)], and complex-coordinate [Ref. 24(f)] quantum formulations. The connections between the three first approaches are given in Refs. 24(c), 24(e), and 24(g).

[21]The importance of such an approximation, at this point, is that by letting the primary photoelectron be completely

decoupled from the intermediate and final states the applicability of the scattering theory, usually formulated for processes where at most one particle is present in one continuum channel, is assured for the auger and x-ray emission processes where, strictly speaking, there exist at least two partices (two electron or one electron and one photon) in the continuum associated to the final ions. Once the final result, here represented by Eq. (11), is achieved a generalization of this resonant-scattering theory for the possibility of two or more particles in one continuum channel is feasible, thereby broadening the domain of this applicability to a family of PCI related processes. For more details on this point we refer the reader to Refs. 1 and 24(e) and 24(g).

[22]B. A. Lippman and J. Schwinger, Phys. Rev. **79**, 469 (1950).

[23]G. Breit and H. A. Bethe, Phys. Rev. **93**, 888 (1954).

[24](a) R. B. Barker and H. W. Berry, Phys. Rev. **151**, 14 (1966); P. J. Hicks, S. Cvejanovic, J. Comer, F. Read, and J. M. Sharp, Vacuum **24**, 573 (1974); V. Schmidt, S. Krummacher, F. Wuilleumier, and P. Dhez, Phys. Rev. A **24**, 1803 (1981); (b) A. Niehaus, J. Phys. B **10**, 1845 (1977); (c) A. Russek and W. Mehlhorn, J. Phys. B **19**, 911 (1986); (d) M. Ya. Amus'ya, M. Yu. Kuchiev, and S. A. Sheĭnerman, Zh. Eksp. Teor. Fiz. **76**, 470 (1979) [Sov. Phys.—JETP **49**, 238 (1979)]; in *Coherence and Correlation in Atomic Collisions,* edited by H. Kleinpoppen and J. F. Williams (Plenum, New York, 1980), p. 297; (e) T. Åberg, in *Inner-shell and X-Ray Physics of Atoms and Solids,* edited by D. J. Fabian, H. Kleinpoppen, and L. M. Watson (Plenum, New York, 1981), p. 251; (f) P. Froelich, O. Goscinski, U. Gelius, and K. Helenelund, J. Phys. B **17**, 979 (1984); (g) J. Tulkki, G. N. Armen, T. Åberg, B. Crasemann, and M. H. Chen, Z. Phys. D **5**, 241 (1987).

[25]L. S. Cederbaum and W. Domcke, J. Chem. Phys. **60**, 2878 (1974); **64**, 603 (1976).

[26]L. S. Cederbaum and W. Domcke, Adv. Chem. Phys. **36**, 205 (1977).

[27]H. Köppel, W. Domcke, and L. S. Cederbaum, Adv. Chem. Phys. **57**, 59 (1984).

[28]H. Ågren and J. Müller, J. Electron Spectrosc. Relat. Phenom. **19**, 285 (1980).

[29]W. Domcke, L. S. Cederbaum, H. Köppel, and W. von Niessen, Mol. Phys. **34**, 1759 (1977).

[30]E. J. Heller, Acc. Chem. Res. **14**, 368 (1981).

[31]E. B. Wilson, J. C. Decius, and P. C. Cross, *Molecular Vibrations* (McGraw-Hill, New York, 1955).

[32]F. Dushinsky, Acta Physicochim. USSR **7**, 551 (1937).

[33]M. Berman, H. Estrada, L. D. Cederbaum, and W. Domcke, Phys. Rev. A **28**, 1363 (1983).

[34]See Sec. IV of this work, and also Refs. 11–16.

[35]D. Neumann and J. W. Moskowitz, J. Chem. Phys. **49**, 2056 (1968).

[36]P. E. M. Siegbahn, J. Chem. Phys. **75**, 2314 (1981).

[37]T. E. Sharp and H. M. Rosenstock, J. Chem. Phys. **41**, 3453 (1964).

[38]A. R. Hoy, I. M. Mills, and G. Strey, Mol. Phys. **24**, 1265 (1972).

[39]J. A. Smith, P. Jørgensen, and Y. Öhrn, J. Chem. Phys. **62**, 1285 (1975).

[40]L. Karlsson, L. Mattson, R. Jadrny, R. G. Albridge, S. Pinchas, T. Bergmark, and K. Siegbahn, J. Chem. Phys. **62**, 4745 (1975).

[41]P. J. Fortune, B. J. Rosemberg and A. C. Wahl, J. Chem. Phys. **65**, 2201 (1976); see also Ref. 46.

[42]J. E. Rubensson, L. Pettersson, N. Wassdahl, M. Bäckström, and J. J. Nordgren, J. Chem. Phys. **82**, 4486 (1985).

[43]D. W. Turner, C. Baker, A. D. Baker, and C. R. Brundle, *Molecular Photoelectron Spectroscopy* (Wiley-Interscience, London, 1970).

[44]R. N. Dixon, G. Duxbury, J. W. Rabalais, and L. Åsbrink, Mol. Phys. **31**, 423 (1976).

[45]L. S. Cederbaum and W. Domcke, Chem. Phys. Lett. **25**, 357 (1974).

[46]C. F. Jackels, J. Chem. Phys. **72**, 4873 (1980).

[47]U. Gelius, E. Basilier, S. Svensson, T. Bergmark, and K. Siegbahn, J. Electron Spectrosc. Relat. Phenom. **2**, 405 (1974).

[48]H. Siegbahn, L. Asplund, and P. Kelfve, Chem. Phys. Lett. **35**, 330 (1975).